Available online at website: https://journal.bcrec.id/index.php/jcerp

Journal of Chemical Engineering Research Progress, 3 (1) 2026, 136-158

Research Article

Development and Optimization of a Laboratory-Scale Bubble Column Bioreactor for Bioethanol Fermentation: A Computational Approach

David Abutu[1,2,4*], Hafizuddin Wan Yussof[1], Benjamin Olufemi Aderemi[2], Alewo Opueda Ameh[4], Augustine Agi[1,3]

[1]*Faculty of Chemical and Process Engineering Technology, Universiti Malaysia Pahang Al-Sultan Abdullah, Lebuhraya Persiaran Tun Khalil Yaakob 26300 Kuantan, Pahang, Malaysia.*

[2]*Department of Chemical Engineering, Ahmadu Bello University Zaria, Nigeria.*

[3]*Centre for Research in Advanced Fluid and Processes (Fluid Centre), Universiti Malaysia Pahang Al-Sultan Abdullah, 26300 Gambang, Pahang, Malaysia.*

[4]*Department of Chemical Engineering, Federal University Wukari, Nigeria.*

Received: 22th January 2026; Revised: 27th February 2026; Accepted: 28th February 2026
Available online: 3rd March 2026; Published regularly: June 2026

Abstract

This study presents the design and optimization of a laboratory-scale bubble column bioreactor (BCB) for bioethanol fermentation. Python-based simulations in Google Colab were employed to analyze mass transfer dynamics, hydrodynamic behavior, and reactor scale-up strategies under varying aeration rates. Although ethanol production is an anaerobic process, oxygen transfer analysis was conducted to characterize reactor performance and establish oxygen-limited conditions suitable for Saccharomyces cerevisiae fermentation, incorporating mass transfer modeling, reaction kinetics, process control, and sparger design to enhance fermentation efficiency. To further enhance fermentation efficiency, Response Surface Methodology (RSM) was applied following a two-stage optimization approach. A working volume of 500 mL was defined using fermentation kinetics, including an oxygen uptake rate of 1.1 g O_2/g cells, biomass yield of 0.5 g/g glucose, and k_La of 50 h^{-1}. A perforated plate sparger with six 1.2 mm orifices achieved a gas velocity of 90.3 m/s and 2.68 mm bubble size. Aeration was dynamically controlled to maintain 0.002 g/L dissolved oxygen, while pH was regulated at 5.0–5.5 using NaOH dosing. These conditions yielded 44.3% ethanol. A full factorial design identified Time, Air Flow Rate, Cell Loading, and Bead Mass as significant factors. RSM with Central Composite Design confirmed a significant quadratic model ($F = 14.14$, $p < 0.0001$; $R^2 = 0.9601$, Adjusted $R^2 = 0.9201$). Cell Loading ($F = 48.48$) and Bead Mass ($F = 26.53$) had the strongest effects. Optimal conditions yielded 47.9% ethanol at 52.70 h, 1.55 L/min air, 1.51 g/L cells, and 47.20 g beads, with 0.84% prediction error.

Keywords: Bubble Column Bioreactor; Optimization; Design; Modelling; Google Co-Lab

How to Cite: David, A., Wan Yussof, H., Aderemi, B. O., Ameh, A. O., Agi, A. A. (2026). Development and Optimization of a Laboratory-Scale Bubble Column Bioreactor for Bioethanol Fermentation: A Computational Approach. *Journal of Chemical Engineering Research Progress*, 3 (1), 136-158 (doi: 10.9767/jcerp.20646)

Permalink/DOI: https://doi.org/10.9767/jcerp.20646

1. Introduction

The global shift toward sustainable energy sources has intensified research into bioethanol production, primarily due to its renewability, carbon neutrality, and potential as a fuel additive [1]. Bioethanol is commonly produced through the fermentation of sugars by yeast, with Saccharomyces cerevisiae being the most widely used microorganism due to its high ethanol yield, robustness, and adaptability to industrial conditions [2]. To optimize bioethanol production, it is crucial to enhance mass transfer efficiency, regulate fermentation parameters, and minimize process limitations, which necessitates the development of efficient bioreactors [3].

Among various bioreactor configurations, the bubble column bioreactor (BCB) has gained

* Corresponding Author.
Email: pcz23024@adab.umpsa.edu.my (D. Abutu)

significant attention due to its high oxygen transfer efficiency, simple design, low energy consumption, and ease of scale-up [4,5]. BCBs operate by introducing air or oxygen in the form of bubbles, which facilitates gas-liquid mass transfer and mixing without requiring mechanical agitation [6]. This feature makes BCBs particularly advantageous for aerobic fermentation processes such as yeast-based ethanol production, where oxygen supply, pH stability, temperature control, and foam management are critical for process optimization [7-9].

To effectively design and optimize a BCB for bioethanol fermentation, computational tools such as Python-based modeling are essential for predicting mass transfer rates, reaction kinetics, and process stability. Google CoLAB simulations enable the evaluation of key parameters such as oxygen uptake rate (OUR), volumetric oxygen transfer coefficient ($k_L a$), glucose consumption rate, ethanol yield, and CO_2 evolution. Proper control of these factors ensures maximum ethanol productivity while preventing process limitations such as oxygen depletion, pH fluctuations, and excessive foam formation [10]. While ethanol production by Saccharomyces cerevisiae occurs optimally under anaerobic or oxygen-limited conditions, understanding the oxygen transfer capacity of a bioreactor is critical during the design phase. Oxygen transfer simulations inform hydrodynamic design, CO_2 stripping behavior, and pre-culture oxygen exposure. Moreover, due to the Crabtree effect, ethanol production can occur even under limited oxygen conditions, particularly during batch processes with high sugar concentrations.

Although bubble column bioreactors have been widely investigated for aerobic bioprocesses, limited studies have integrated oxygen transfer modeling with oxygen-limited ethanol fermentation design in a laboratory-scale system. Furthermore, previous works often treat hydrodynamic design, kinetic modeling, and statistical optimization as separate steps rather than a unified computational framework. This study presents the design, simulation, and optimization of a laboratory-scale BCB (500 mL) for bioethanol fermentation, incorporating oxygen transfer modeling, dynamic aeration control, pH stabilization, temperature regulation, foam suppression and response surface methodology. The novelty of this work lies in the development of an integrated Python-based computational platform that simultaneously couples mass transfer analysis, fermentation kinetics, sparger design, and multivariable optimization prior to reactor fabrication. The Python-based computational framework allows for the prediction of glucose consumption, biomass growth, and bioethanol synthesis, providing a scalable model for industrial bioethanol process development. Additionally, the implementation of a two-stage optimization strategy (factorial screening followed by RSM) within the same modeling environment provides a systematic pathway from conceptual design to statistically validated operating conditions. Based on these simulations, the reactor was subsequently fabricated for experimental validation and future scale-up applications

2. Materials and Method

2.1 Process Design Assumptions

The following assumptions were made to simplify the design calculations and ensure the feasibility of scale-up. The system was assumed to operate under steady-state conditions with stable fermentation parameters [11], and uniform mixing was considered to ensure consistent environmental conditions throughout the reactor. Cell flocculation was assumed negligible to prevent sedimentation, and the bioreactor volume was considered constant with minimal liquid loss. The initial glucose concentration was fixed at 50 g/L to ensure sufficient carbon availability for yeast growth. The yeast oxygen requirement was estimated at 1.1 g O_2/g biomass to sustain aerobic metabolism [12], while glucose consumption under optimal conditions was assumed to occur at a rate of 2 g/L·h [12]. The reactor was assumed to experience 15% gas holdup (ϵ_g = 0.15), thereby reducing the effective liquid volume [14].

Oxygen transfer was described using film theory, where the driving force is defined as the difference between the saturated dissolved oxygen concentration and the actual oxygen level in the medium [15]. A minimum dissolved oxygen concentration of 0.002 g/L was required to prevent oxygen limitation [12]. Yeast growth kinetics were modeled using the Monod equation with a maximum specific growth rate of 0.3 h^{-1} [16] and a substrate affinity constant (K_s) of 1 g/L, indicating that growth rate depends on glucose concentration [17]. The biomass yield on glucose ($Y_x/_s$) was taken as 0.5 g cells/g glucose, meaning that 50% of glucose is converted into biomass [13], [18]. The ethanol yield on glucose ($Y_p/_s$) was assumed to be 0.48 g ethanol/g glucose, reflecting that bioethanol production is a secondary process under aerobic conditions [19]. Carbon dioxide evolution ($YCO_2/_s$ = 1.0 g/g glucose) was included to model gas formation and foam generation [20].

The pH was maintained between 5.0 and 5.5 using an automated NaOH buffering system [21-22], and when the pH dropped below 5.0, NaOH was automatically added to restore the optimal range. Yeast metabolism was assumed to generate 15 kJ of heat per gram of biomass

(YQ/X), contributing to an increase in medium temperature [23]. Foam formation was modeled based on CO_2 and ethanol production rates [24], and when foam volume exceeded 10% of the reactor height, antifoam agents were automatically dosed [24]. The governing equations for biomass growth, ethanol production, and process control were solved using the Runge–Kutta numerical integration method [25-28]. Finally, the system was simulated for 48 hours to evaluate long-term fermentation performance [29]. Figure 1 presents a schematic overview of the integrated computational approach adopted in this study. The framework combines hydrodynamic modelling, mass transfer evaluation, reaction kinetic simulation, and process optimization to systematically analyse and enhance the performance of the bubble column bioreactor.

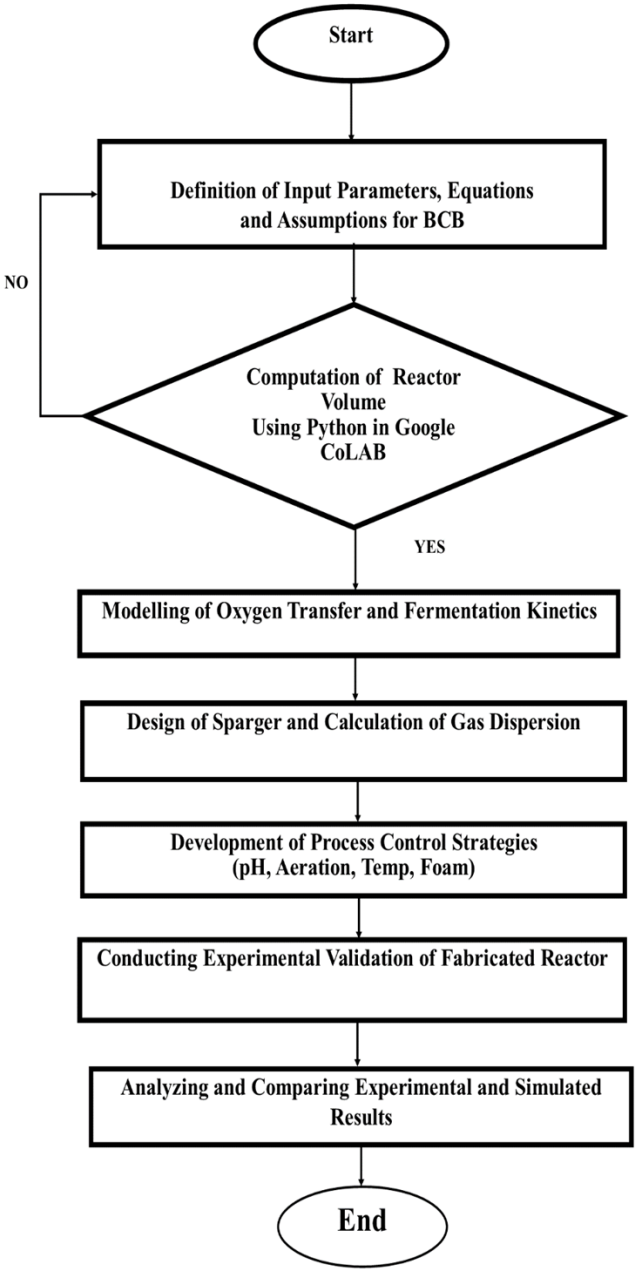

Figure 1. Flow chart of the integrated computational framework for hydrodynamic modeling, mass transfer analysis, kinetic simulation, and process optimization of the bubble column bioreactor.

2.2 Determination of Reactor Volume Using the Equation of State

The working volume of the bubble column bioreactor (BCB) was determined using an equation of state for fermentation processes involving immobilized yeast cells [30]. The reactor volume (V) was computed based on mass transfer, oxygen uptake, and glucose consumption kinetics [31]. In a bubble column fermenter, oxygen transfer occurs through the Gas phase (bubbles rise through the liquid) and Liquid phase (oxygen dissolves and is consumed by yeast). Equations (1-33) describes the equation of state and kinetic expression of the bubble column fermenter [31-32]. Python code for the design calculation is presented in the supplementary file attached.

At steady state, the oxygen input via bubbles equals oxygen consumption by yeast:

Oxygen input = Oxygen transfer = Oxygen consumption

$$F_{O_2} . C_{O_2,in} = k_L a . V . \left(C_{O_{2^*}} - C_{O_2}\right) = V . rO_2 \quad (1)$$

Since yeast consumes oxygen based on glucose uptake, substituting r_{O2}:

$$V = \frac{F_{O_2} . C_{O_2,in}}{Y_{O_2/X} . Y_{X/S} . r_S} \quad (2)$$

2.3 Bubble Column Oxygen Transfer Rate

In a bubble column, oxygen dissolves through gas-liquid mass transfer:

$$rO_2 = k_L a . \left(C_{O_{2^*}} - C_{O_2}\right) \quad (3)$$

For steady state:

$$k_L a . \left(C_{O_{2^*}} - C_{O_2}\right) = Y_{O_2/X} . Y_{X/S} . r_S \quad (4)$$

Solving for V:

$$V = \frac{F_{O_2} . C_{O_2,in}}{k_L a . \left(C_{O_{2^*}} - C_{O_2}\right)} \quad (5)$$

Since oxygen solubility follows Henry's Law: Substituting C_{O2*} :

$$V = \frac{F_{O_2} . C_{O_2,in}}{k_L a . \left(\frac{P_{O_2}}{H} - C_{O_2}\right)} \quad (6)$$

Incorporating bubble column gas holdup: in a bubble column, gas holdup ε_g represents the fraction of reactor volume occupied by gas bubbles:

$$V_L = V\,(1 - \varepsilon_g) \tag{7}$$

$$rO_2 = Y_{O_2/X} \,.\, Y_{X/S} \,.\, r_S \tag{8}$$

$$C_{O_2*} = \frac{P_{O_2}}{H} \tag{9}$$

Thus, correcting for the effective liquid volume:

$$V_L = \frac{F_{O_2} \,.\, C_{O_2,in}}{k_L a\,(1-\varepsilon_g)\left(\frac{P_{O_2}}{H} - C_{O_2}\right)} \tag{10}$$

Final equation of state for a bubble column fermenter: however, in a semi-batch system, the oxygen mass balance changes over time:

$$\frac{dCO_2}{dt} = k_L a \,.\left(C_{O_2*} - C_{O_2}\right) - \frac{r_{O_2}(t)}{X} \tag{11}$$

$$\frac{dCO_2}{dt} = \text{Change in dissolved oxygen over time} \tag{12}$$

$$r_{O_2}(t) = \text{Time} - \text{dependent oxygen uptake rate} \tag{13}$$

$$V_L = \frac{F_{O_2}\, Y_{O_2/X} \,.\, Y_{X/S} \,.\, r_S}{k_L a\,(1-\varepsilon_g)\left(\frac{P_{O_2}}{H} - C_{O_2}\right)} \tag{14}$$

2.4 Bioreactor Design and Computational Modeling

A Google CoLAB-based computational framework was employed to simulate oxygen transfer, reaction kinetics, and overall process dynamics within the BCB. The reactor was configured as a gas-liquid contactor equipped with a perforated plate sparger to ensure efficient gas dispersion. The mathematical formulation of the system is governed by Equations (1–14), which describe the hydrodynamic behavior, mass transfer mechanisms, and reaction kinetics incorporated into the model.

2.5 Oxygen Mass Transfer

2.5.1 Oxygen transfer modeling purpose

Oxygen transfer modeling was conducted not to simulate aerobic ethanol production, but to characterize the reactor's hydrodynamic performance under different flow regimes. Parameters such as the oxygen transfer rate (OTR) and oxygen uptake rate (OUR) were calculated to estimate reactor volume, gas holdup, and dynamic aeration needs prior to switching to oxygen-limited conditions. These metrics are routinely used in fermenter design, even when operating conditions are anaerobic [47-48].

$$OTR = k_L a \,.\left(C_{O_2*} - C_{O_2}\right) \tag{15}$$

2.5.2 Fermentation kinetics

Biomass growth was modeled using the Monod equation:

$$\mu = \frac{\mu_{max} S}{K_s + S} \tag{16}$$

where, μ_{max} is the maximum specific growth rate (0.3 h^{-1}) and K_s is the substrate affinity constant (1 g/L). Glucose consumption followed first-order kinetics:

$$S\,(t) = S_o \,.\, e^{-r_s.t} \tag{17}$$

2.5.3 Sparger design

The sparger is a crucial component of the bubble column bioreactor (BCB), facilitating gas dispersion, oxygen transfer, and mixing within the fermentation medium [33]. Its design affects key parameters such as bubble size and distribution, which influence mass transfer efficiency, gas holdup and residence time, impacting oxygen availability for microbial growth, and pressure drop, determining energy consumption for aeration. Common sparger types include orifice spargers (perforated plates) for uniform gas distribution with moderate pressure drop, porous spargers for fine bubbles and high oxygen transfer but increased pressure drop, and ring or cross spargers for even gas dispersion. For this 500 mL laboratory-scale BCB, a perforated plate sparger is chosen due to its simple fabrication, uniform bubble dispersion, and moderate pressure drop. The sparger was designed as a perforated plate with six orifices of 1.2 mm diameter, ensuring uniform gas dispersion. The design calculations for the sparger uses Equations (18-24). The Python code for solution to the equation is presented in the supplementary file attached.

Total Gas Flow Rate (Q_g):

$$Q_g = \frac{V.OUR}{(C_{O_2*} - C_{O_2})} \tag{18}$$

Orifice Diameter (d_o):

$$Q_g = \sqrt{\frac{2\Delta P}{\rho g}} \tag{19}$$

$$Q_g = N.A_o v_o \tag{20}$$

$$d_o = \sqrt{\frac{4Q_g}{\pi N v_o}} \tag{21}$$

Sparger Pressure Drop (ΔP):

$$\Delta P = \left(\frac{1}{C_d}\right)^2 \times \frac{\rho_g v_o^2}{2} \tag{22}$$

Bubble Size and Rise Velocity (d_b):

$$d_b = 1.36 \times (\frac{\sigma}{\rho l g})^{1/3} \quad (23)$$

Bubble rise velocity is estimated using Stokes' Law:

$$v_b = \frac{2}{9} \times \frac{(\rho_l - \rho_g) g d_b^2}{\mu} \quad (24)$$

2.6 Process Control Strategies

Dynamic aeration control: the oxygen flow rate was dynamically adjusted based on real-time oxygen uptake rate (OUR) and oxygen transfer rate (OTR) using:

$$F_{O_2}(t) = F_{O_2,init} \times (1 + \frac{OUR - OTR}{OTR}) \quad (25)$$

pH regulation: a buffering system was used to maintain pH within 5.0–5.5 through automated NaOH dosing:

$$pH\ (t) = pH_o - kCO_2 . CO_2(t) \quad (26)$$

Temperature and foam control: heat generation from microbial metabolism was modeled as:

$$Q = Y_{Q/X} . X \quad (27)$$

Aeration power requirement: the power required for aeration in a bubble column is estimated using:

$$P = \frac{F_{O_2} . \rho_g . g . H_t}{\eta} \quad (28)$$

Glucose depletion over time: glucose is consumed based on first-order kinetics:

$$S\ (t) = S_o . e^{-r_s . t} \quad (29)$$

Biomass growth over time: biomass follows an exponential growth model:

$$X\ (t) = X_o . e^{\mu . t} \quad (30)$$

Oxygen Uptake Rate (OUR): determines how much oxygen yeast consumes per unit of biomass:

$$r_{O_2} = Y_{O_2/X} . X\ (t) \quad (31)$$

Substrate yield efficiency ($Y_{S/X}$): indicates how efficiently glucose is converted into biomass:

$$Y_{S/X} = \frac{S_{consumed}}{X\ (t) - X_o} \quad (32)$$

Gas flow optimization (Oxygen Transfer Rate, OTR): compares oxygen uptake rate (OUR) and oxygen transfer rate (OTR) to check if oxygen supply is sufficient:

$$OTR = k_L a . (C_{O_2 *} - C_{O_2}) \quad (33)$$

2.7 Python Code Simulation and Experimental Validation

The computational model was implemented in Google CoLab using Python and validated against literature data. The system of differential equations was solved using the Runge-Kutta numerical integration method over a 48-hour fermentation period [34]. The fabricated reactor, constructed from stainless steel fittings, was experimentally tested for gas dispersion efficiency, oxygen transfer, and process stability [31]. Results demonstrated strong agreement between simulated and experimental values, confirming the robustness of the model for future scale-up applications.

2.8 Bioreactor Design and Computational Framework

The bubble column bioreactor was designed to facilitate oxygen mass transfer, substrate utilization, and process stability. A Google Co-Lab-based computational model was developed to simulate key fermentation parameters and optimize process conditions.

2.9 Fabrication of the Reactor

The fabrication of the laboratory-scale bubble column bioreactor (BCB) was based on the computed reactor volume of 500 mL, ensuring an optimal aspect ratio for efficient gas-liquid mass transfer. The reactor was constructed using stainless steel to provide durability, chemical resistance, and ease of sterilization, making it suitable for bioethanol fermentation. Based on the calculated working volume, the reactor was designed with a height of 70 cm and a diameter of 3.02 cm, maintaining an aspect ratio which enhances bubble dispersion, oxygen transfer, and fermentation efficiency.

An air rotameter was installed to regulate the airflow rate within the column, ensuring controlled oxygen supply. A mini air compressor was sized based on the calculated aeration power requirement (0.006 W) to provide sufficient gas flow for effective mass transfer. Pressure sensors were incorporated to monitor system pressure, preventing over-aeration, and maintaining process stability. A temperature controller was integrated to regulate the fermentation temperature to 35 °C, by circulating hot water, preventing heat-induced yeast inhibition. The fabricated reactor was tested using a 5 g/L glucose solution with immobilized *Saccharomyces cerevisiae*, and key operational parameter such as ethanol yield were evaluated. Further drawings

and picture of the experimental setup is shown in Figure S1-S5 of the supplementary file.

2.10 Optimization of Process Parameter for the Bubble Column Bioreactor

2.10.1 Materials

Ferric chloride with purity of 99%, glutaraldehyde, acetic acid (99%), calcium chloride, 3,5-Dinitrosalicylic acid (DNS) and chitosan with molecular weight of 4.9×10^5 and degree of deacetylation of 85% were purchased from Sigma Aldrich. Ferrous chloride with purity of 98% was obtained from Thermo Fisher. Sodium acetate with molecular weight of 82.03g/mol was supplied by Merck. Ammonium hydroxide (NH_4OH, 25% v/v) was obtained from Fisher Scientific. Sodium hydroxide (NaOH) with molecular weight of 39.9 g/mol was purchased from Alfa Aesar. Sodium alginate with average molecular weight of 2.4×10^5 was gotten from FMC BioPolymer. *Saccharomyces Cerevisiae* (strain SCY026) was obtained from Nanjing Tessin Biotechnology Co., Ltd. China.

2.10.2 Experimental design approach

A two-stage statistical design methodology was employed to optimize ethanol fermentation in a 500 mL bubble column bioreactor using *Saccharomyces cerevisiae* immobilized on iron oxide nanoparticle-modified calcium alginate beads. The study initially utilized a factorial design of experiments (DOE) to evaluate the effects of seven independent factors temperature, pH, substrate concentration, fermentation time, gas flow rate, mass of immobilization beads, and cell loading on supports on ethanol yield. The results from the factorial analysis were used to construct a Pareto chart, identifying the three most statistically significant factors covering biological (yeast activity and immobilization), chemical (substrate concentration and pH), and reactor hydrodynamic properties (gas flow rate and mass transfer efficiency). These parameters were subsequently optimized using a Central Composite Design (CCD) within Response Surface Methodology (RSM) to establish optimal conditions for enhanced ethanol production [35-37].

2.10.3 Factorial experimental design

A full 2^7 factorial design was employed to assess the main and interaction effects of the seven selected parameters. Each factor was evaluated at three levels: low (-1), medium (0), and high (+1), ensuring a comprehensive experimental space (Table 1). The factorial experiment comprised 32 randomized trials with replicates to improve statistical accuracy. Ethanol yield was designated as the response variable, and data were analyzed using Analysis of Variance (ANOVA). A Pareto chart was used to rank the significance of each parameter based on its impact on ethanol yield. The three most influential factors identified were selected for further optimization using CCD [38-39].

2.10.4 Optimization using Central Composite Design (CCD)

The three most significant factors identified from the factorial analysis were optimized using CCD within RSM, which provides a robust framework for modeling quadratic interactions and optimizing nonlinear responses. The CCD included axial points (±α), factorial points (-1, +1), and central points (0,0), resulting in a total of 30 experimental runs, sufficient to capture second-order polynomial effects. A quadratic regression model was developed to describe ethanol yield as a function of the selected process parameters. Model adequacy was assessed using ANOVA, coefficient of determination (R^2), lack-of-fit tests, and residual diagnostics. Optimization was carried out using response surface plots and desirability function analysis to determine the ideal fermentation conditions that maximize ethanol yield while minimizing residual glucose concentration. The second order polynomial model is represented as shown in Equations (34-36) [40]:

Table 1. Variation of parameter for six (7) numerical factors [41-43].

Variable	Low level (-1)	High level (+1)
Time (h)	24	96
Substrate Concentration (g/L)	50	200
Cell loading (OD600 Value)	1	5
Mass of immobilized bead (g)	10	50
Temperature (^oC)	25	40
pH	4.5	5.5
Air Flow rate (L/min)	0.5	2.5

$$Y = \beta_0 + \sum_{i=1}^{n} \beta_i X_i + \sum_{i=1}^{n} \beta_{ii} X_i^2 + \sum_{i=1}^{n} X \sum_{i=1}^{n} \beta_{ij} X_i X_j + \epsilon \quad (34)$$

where Y represents ethanol yield, X_i are the independent variables, and β_0, β_i, β_{ii}, β_{ij} are regression coefficients. Model adequacy was validated using ANOVA, coefficient of determination (R^2), and lack-of-fit tests:

$$R^2 = 1 - \frac{\Sigma(Y_{exp} - Y_{pred})^2}{\Sigma(Y_{exp} - \bar{Y})^2} \quad (35)$$

A non-significant lack-of-fit test indicated a well-fitted model:

$$F_{LOF} = \frac{Mean\ Square\ Lack\ of\ Fit}{Mean\ Square\ Pure\ Error} \quad (36)$$

The optimal fermentation conditions were predicted using response surface plots and desirability function analysis and validated through confirmatory experiments.

2.10.5 Bioreactor Setup and Fermentation Conditions

All fermentation experiments were conducted in a custom-designed 500 mL bubble column bioreactor as shown in Figure 2. The bioreactor was operated under batch mode, with a working volume of 400 mL, allowing sufficient headspace for gas-liquid interactions. The immobilization beads, consisting of iron oxide nanoparticle-modified calcium alginate, were introduced at predefined concentrations to facilitate cell retention and enhance metabolic activity. The fermentation medium contained glucose (50–200 g/L) as the primary carbon source, supplemented with yeast extract (5 g/L), ammonium sulfate (2 g/L), magnesium sulfate (0.5 g/L), and potassium phosphate buffer (2 g/L). The pH was adjusted within the experimental range using 1 M HCl and 1 M NaOH solutions.

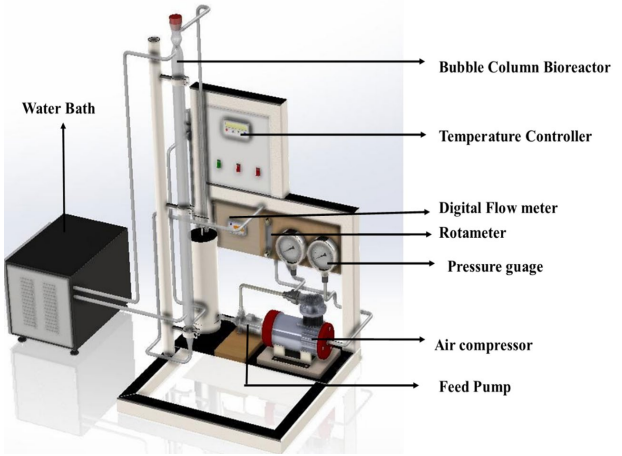

Figure 2. Schematic representation of the bubble column bioreactor.

Gas flow rate was controlled using a precision rotameter (0.5–2.5 L/min), and temperature was maintained via a thermostatically controlled water jacket.

2.10.6 Bead preparation and immobilization procedure

The immobilization beads were prepared by ionic gelation of calcium alginate (2% w/v) crosslinked with $CaCl_2$ (0.1 M), incorporating iron oxide nanoparticles (Fe_3O_4) at 0.5% (w/v). The modified beads were synthesized by dispersing Fe_3O_4 nanoparticles (<50 nm particle size) into the alginate solution under constant stirring, followed by extrusion into a $CaCl_2$ bath using a peristaltic pump with a nozzle diameter of 0.5 mm to ensure uniform bead size (~2 mm in diameter). Immobilized *S. cerevisiae* was introduced at varying concentrations based on optical density at 600 nm (OD600, range: 1.0–4.0). The beads were hardened for 1 hour, washed with sterile saline, and stored at 4 °C before use.

2.10.7 Analytical methods

Fermentation samples were collected at predetermined intervals for ethanol and glucose quantification. Ethanol concentration was measured using high-performance liquid chromatography (HPLC, Agilent 1260 Infinity) equipped with a refractive index detector (RID) and an Aminex HPX-87H column (Bio-Rad, USA), operated at 65 °C with 5 mM sulfuric acid as the mobile phase (0.6 mL/min flow rate). Glucose concentration was determined using a glucose oxidase-peroxidase (GOD-POD) enzymatic assay kit. Yeast viability within the immobilized beads was assessed using colony-forming unit (CFU) counts after bead dissolution in sodium citrate (0.1 M). Ethanol yield was calculated based on equation 37. The theoretical ethanol yield (0.51 g ethanol/g glucose) was used to determine fermentation efficiency (η) as shown in Equation (38).

$$Y_{e/s} = \frac{C_e}{C_s} \quad (37)$$

where, C_e is the final ethanol concentration (g/L) , C_s *is* the glucose consumed (g/L).

$$\eta = \frac{Y_{e/s}}{0.51} \times 100 \quad (38)$$

2.10.8 Statistical analysis and model validation

All experimental data were analyzed using Design-Expert® software (Stat-Ease Inc., USA). Factorial analysis was conducted using ANOVA, identifying significant factors through p-values (≤0.05) and effect estimates. For CCD, regression

coefficients were estimated, and response surface plots were generated to visualize interaction effects. The final optimization model was validated by conducting confirmatory experiments under the predicted optimal conditions, comparing experimental ethanol yields to model predictions using percent error analysis.

3. Results and Discussion

3.1 Design of the Bubble Column Fermenter

Fermentation experiments were performed under oxygen-limited conditions. After an initial biomass buildup period, the reactor was sparged with nitrogen to reduce the dissolved oxygen level. Dissolved oxygen was maintained below 0.2 mg/L throughout fermentation. This ensured that ethanol synthesis occurred under microaerobic conditions typical of batch ethanol fermentations.

The calculated parameters for the bubble column bioreactor and the sparger as shown in Table 2 and Table 3 ensure optimal reactor performance by balancing oxygen transfer, gas dispersion, and microbial growth. The oxygen transfer coefficient (k_La) of 50 h^{-1} aligns well with literature values for effective oxygenation in aerobic fermentation. Studies have shown that optimal oxygen transfer coefficients generally range from 45 to 60 h^{-1}, depending on system configurations and microbial oxygen demands [44]. For instance, a study on high-density fermentation of *Spathaspora passalidarum* demonstrated peak ethanol volumetric productivity at a k_La of 45 h^{-1}, reducing fermentation time significantly [45]. The reactor volume of 500 mL was chosen based on mass transfer efficiency and oxygen uptake demands to ensure a scalable design. A comparative study on oxygen mass transfer in different bioreactor scales suggested that maintaining a consistent k_La across different volumes is key to ensuring predictable scale-up outcomes [46]. In a pilot-scale fermentation system, it was found that maintaining a similar k_La between 5 L and 50 L fermentors allowed for consistent microbial growth and product yield [46].

The sparger design, with six orifices of 1.2 mm diameter, provides a bubble diameter of 2.68 mm, optimizing gas-liquid mass transfer. The design considerations align with findings that emphasize the importance of sparger geometry in determining shear conditions and gas dispersion efficiency [47]. Studies indicate that sparger designs with multiple smaller orifices produce finer bubbles, increasing surface area for oxygen transfer and improving k_La [48]. Compared to perforated plate spargers, membrane-tube spargers have been shown to improve gas dispersion efficiency by up to 48% [48]. The pressure drop across the sparger (14 kPa) ensures sufficient gas penetration while avoiding excessive turbulence. Excessively high gas velocities can lead to shear stress-induced cell damage, particularly in mammalian cell cultures, where gas entrance velocities above 60 m/s have been shown to negatively affect viability [49]. The balance between adequate gas penetration and avoiding excessive shear forces is critical to reactor performance.

These design parameters, validated against computational and experimental data, demonstrate the feasibility of the system for bioethanol fermentation at both laboratory and industrial scales. Computational fluid dynamics (CFD) studies have shown that optimizing impeller-sparger interactions significantly enhances gas dispersion [50]. Furthermore, maintaining appropriate k_La levels in large-scale fermentations ensures product consistency and scalability [46]. Future research will explore further optimizations in gas dispersion efficiency and process scalability, integrating real-time control mechanisms to enhance fermentation performance in large-scale applications.

Table 2. Summary of calculated parameters.

Parameter	Value
Reactor Volume (V)	500 mL
Oxygen Transfer Coefficient (k_La)	50 h^{-1}
Oxygen Uptake Rate (OUR)	1.1 g O_2/g cells
Biomass Yield ($Y_{X/S}$)	0.5 g cells/g glucose
Glucose Consumption Rate (r_S)	2 g/L·h
Gas Flow Rate (Q_g)	2.2 L/h
Gas Holdup Fraction ε	0.15
Orifice Diameter (d_o)	1.2 mm
Number of Orifices (N)	6
Bubble Diameter (d_b)	2.68 mm
Gas Velocity Through Orifice (v_o)	90.3 m/s
Pressure Drop Across Sparger (ΔP)	14 kPa

Table 3. Parameters for the sparger used in the bubble column bioreactor for the fermentation process.

Parameter	Value
Gas Flow Rate (Q_g)	2.2 L/h
Orifice Diameter (d_o)	1.2 mm
Number of Orifices (N)	6
Gas Velocity Through Orifice (v_o)	90.3 m/s
Pressure Drop (ΔP)	13.9kPa
Bubble Diameter (d_b)	2.68mm
Bubble Rise Velocity (v_b)	0.18 m/s

Developing adaptive sparger configurations and aeration strategies tailored for specific bioprocessing conditions can further improve oxygen transfer efficiency [51]. Additionally, real-time monitoring of oxygen mass transfer rates will allow for dynamic adjustments to maintain optimal conditions throughout the fermentation process.

Figure 3 (a) illustrates the glucose consumption trend throughout the fermentation process. The curve typically exhibits an exponential decay pattern, consistent with first-order substrate consumption kinetics. At the initial stages, glucose concentration remains high, but as yeast biomass increases, glucose is rapidly metabolized, leading to a steep depletion. Similar trends have been observed in previous studies, where glucose depletion directly correlates with ethanol production and cell growth [33]. The observed decline aligns with standard fermentation models for *Saccharomyces cerevisiae*, indicating efficient substrate utilization.

However, after an extended period, the rate of glucose depletion gradually slows as yeast cells reach stationary phase due to substrate exhaustion or ethanol accumulation. A study by Pino et al. (2018) reported similar trends in bubble column bioreactors, where a faster glucose depletion rate was linked to increased aeration and oxygen transfer efficiency [52]. This highlights the need for process monitoring and control to optimize fermentation time and yield.

Figure 3 (b) displays the biomass concentration trend throughout fermentation. Initially, biomass remains low, as cells undergo an adaptation (lag phase). As glucose becomes available, biomass enters the exponential growth phase, where the growth rate is dictated by the Monod equation. The figure shows a logarithmic increase in biomass during the mid-phase, aligning with literature reports on bubble column bioreactors, where oxygen transfer efficiency and glucose concentration play a major role in cell proliferation [7].

At later stages, biomass plateaus, indicating that cells have entered the stationary phase, where substrate depletion, ethanol accumulation, and oxygen limitation begin to restrict growth. This trend was similarly observed in microbial fermentation models, where optimal aeration rates were required to sustain prolonged cell activity [10].

Figure 3(c) highlights the simultaneous production of ethanol and CO_2, reflecting yeast metabolism during glucose fermentation. As glucose is consumed, ethanol production steadily increases, reaching a maximum point before leveling off due to product inhibition. The observed ethanol yield ($Y_{P/S}$ = 0.48 g/g) is consistent with results from similar bubble column bioreactor studies [53]. CO_2 production

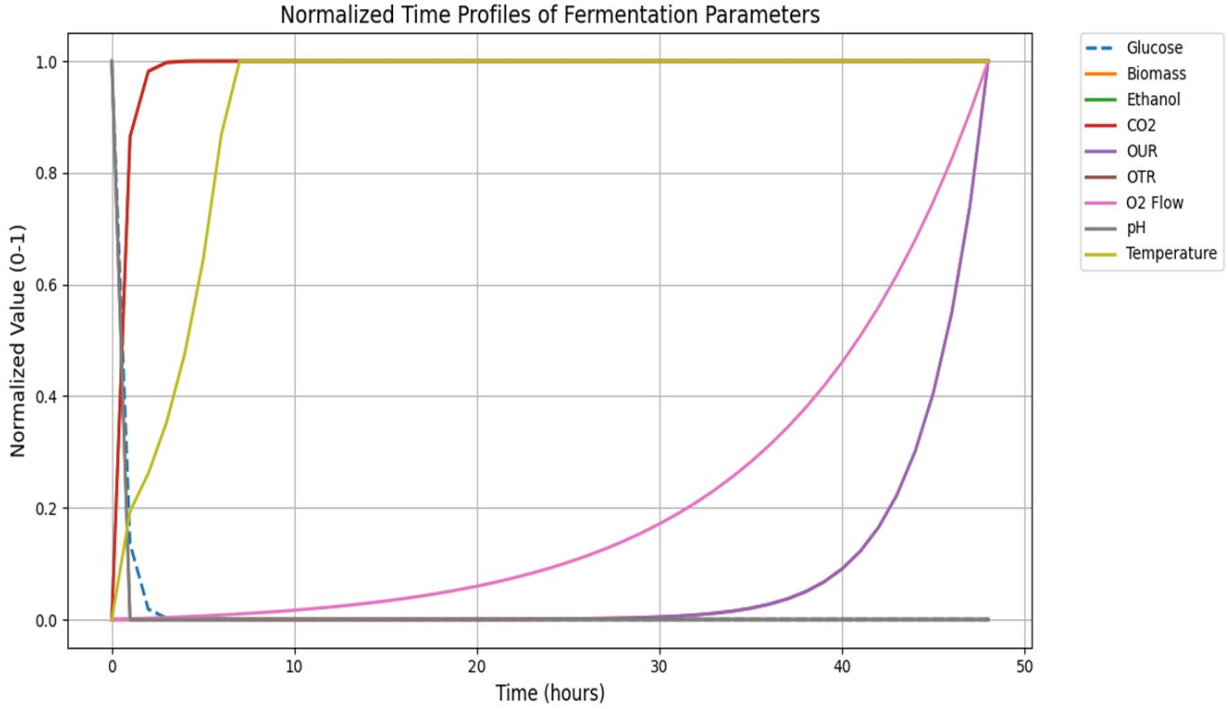

Figure 3. (a) Glucose depletion over time (b) biomass growth over time (c) Ethanol and CO_2 production over time (d) Oxygen uptake rate (OUR) over time (e) Substrate yield efficiency over time (f) Oxygen transfer rate (OTR) over time (g) Dynamic oxygen flow rate over time (h) Biomass production over time with peak biomass time (i) pH correction with NaOH over time (j) Temperature control over time.

follows a similar trajectory, confirming its direct link to ethanol synthesis. Studies on syngas fermentation and microbial ethanol production have demonstrated that CO_2 stripping techniques can improve fermentation efficiency by removing product inhibition effects [54,55].

Oxygen uptake rate (OUR) is a critical parameter in aerobic fermentation, as it influences cell metabolism and ethanol yield. Figure 3(d) shows an initial increase in OUR, corresponding to exponential biomass growth, where oxygen demand is highest. OUR stabilizes as biomass reaches a stationary phase [33]. A decline in OUR towards the end of fermentation suggests oxygen limitation or substrate depletion, requiring process optimization through controlled aeration [53].

Figure 3(e) describes the efficiency of glucose-to-biomass conversion. Initially, yield efficiency is high, reflecting efficient substrate utilization. However, as fermentation progresses, a declining trend is observed, indicating substrate limitation or ethanol inhibition. This trend aligns with bubble column reactor studies, where yield efficiency fluctuates based on oxygen transfer and glucose availability [56]. Figure 3(f) shows that OTR initially increased during the exponential growth phase due to rising microbial oxygen demand, peaking as biomass reached its maximum. As seen in Figure 3 (g), dynamic oxygen flow rate adjustments helped maintain an optimal balance between OTR and oxygen uptake rate (OUR), preventing oxygen limitation. Similarly, Figure 3 (h) highlights biomass production trends, with peak biomass corresponding to maximum oxygen consumption, after which growth slowed due to substrate depletion or metabolic shifts. These findings align with previous studies emphasizing the importance of balancing OTR and OUR to sustain efficient fermentation [57].

pH variation over time, depicted in Figure 3(i), reflected microbial metabolic activity, with an initial drop due to acid production followed by stabilization through NaOH buffering, maintaining pH between 5.0 and 5.5 ensured enzyme stability and optimal yeast performance, preventing growth inhibition caused by excessive acid accumulation. Similarly, Figure 3(j) illustrates temperature regulation at 35 °C, which played a crucial role in sustaining microbial viability and fermentation efficiency while minimizing the risk of thermal stress. These findings are consistent with previous research highlighting the significance of pH and temperature control in fermentation processes [58]. Effective pH correction and temperature stability contributed to maintaining a favorable environment for continuous metabolic activity.

Foam control was essential to prevent process disruptions, with foam levels maintained below 10% of the reactor height using antifoam agents and mechanical defoaming strategies. Excessive foam formation can interfere with oxygen transfer, sensor accuracy, and overall process efficiency. By implementing timely foam control measures, the fermentation process remained stable, allowing consistent oxygen transfer and biomass accumulation. Overall, the integration of dynamic aeration, pH regulation, temperature control, and foam management ensured an optimized fermentation process, maximizing productivity while minimizing potential operational challenges [59].

3.2 Performance Test of the Bubble column bioreactor

The experimental setup consists of a bubble column bioreactor, designed, and fabricated based on simulation data presented in Figure 2. The bioreactor comprises a tubular jacketed glass column, an air supply system powered by a mini compressor, a glucose feed pump, a digital pressure gauge, an air rotameter, a temperature indicator, and a water heater. The reactor, with a total volume of 500 mL, was utilized to study the fermentation of glucose using immobilized *Saccharomyces cerevisiae*. Table 4 shows the performance test carried out for the fermentation of glucose, the average yield of ethanol base on three experimental run is 44.3%. glucose and ethanol concentration were determined using HPLC.

3.3 Comparative Evaluation and Contextualization of Ethanol Yield

The ethanol yield of 44.3% (g ethanol/g glucose) obtained in this study is consistent with yields reported for *Saccharomyces cerevisiae* in batch-mode fermentation systems. For instance, Gonzalez et al., (2022) reported an increase in ethanol yield from 0.41 to 0.43 g/g glucose in a packed-bed tapered-column bioreactor under microaerobic conditions [60]. Similarly, Scriputom et al. [61] achieved comparable yields in a stirred-tank bioreactor using CO_2 stripping, with ethanol concentrations reaching up to 60.3 g/L. A study using hydrothermally pretreated wheat straw with *Saccharomyces cerevisiae* in a 3 L bubble column reactor reported an ethanol concentration of 9.31 g/L using simultaneous saccharification and fermentation (SSF) [60]. However, the strength of the present work lies not merely in the yield but in the computational–experimental workflow that underpins the reactor design and optimization strategy. By integrating a Python-based dynamic simulation which models

substrate consumption, biomass growth, ethanol production, and gas liquid mass transfer with Response Surface Methodology (RSM) for empirical optimization, a modular, predictive, and resource-efficient approach for lab-scale bioethanol process development. Unlike traditional methods that rely on repeated empirical tuning, this framework enables rapid design space exploration and process insight with minimal experimental overhead. While the current BCB system achieved moderate productivity under batch operation, its low energy demand, absence of mechanical agitation, and effective coupling of computational design with statistical optimization offer a scalable and replicable framework for early-stage reactor development.

3.4 Bead Preparation

The digital photographs as shown in Figure 4 of the prepared modified calcium alginate beads as support for the immobilization of saccharomyces cerevisiae. The images clearly show that the beads have a spherical shape and are roughly 3 mm diameter. Upon surface modification with Fe_2O_3 nanoparticles, the Calcium alginate bead turned dark brown in colour.

3.5 Selection of Factors Affecting Ethanol Yield Using Factorial Design

The Pareto chart is a crucial statistical tool used in factorial experimental design to rank the influence of independent variables on a response variable in this case, ethanol yield (%). The principle follows the Pareto rule (80/20 rule), where a small number of factors contribute to the most significant variation in the response (Jia et al., 2020). The Pareto chart shown in Figure 5 and Figure 6 illustrates the standardized effects of seven independent variables on ethanol yield, evaluated against the Bonferroni limit (3.4558) and the t-value threshold (2.0395) to determine statistical significance. Factors with standardized effects above the t-value threshold are considered statistically significant contributors to ethanol yield, while those exceeding the Bonferroni limit are highly significant at a stricter confidence level. In this analysis, none of the factors surpass the Bonferroni limit, indicating that while they influence ethanol yield, their effects are moderate in significance. However, four factors Time (h), Air Flow Rate (L/min), Cell Loading (OD600), and Mass of Bead (g) exceed the t-value threshold (2.0395) confirming their statistical significance for Response Surface Methodology (RSM) using Central Composite Design (CCD). Figure 5 illustrate the contribution of each factor to ethanol yield in the factorial design.

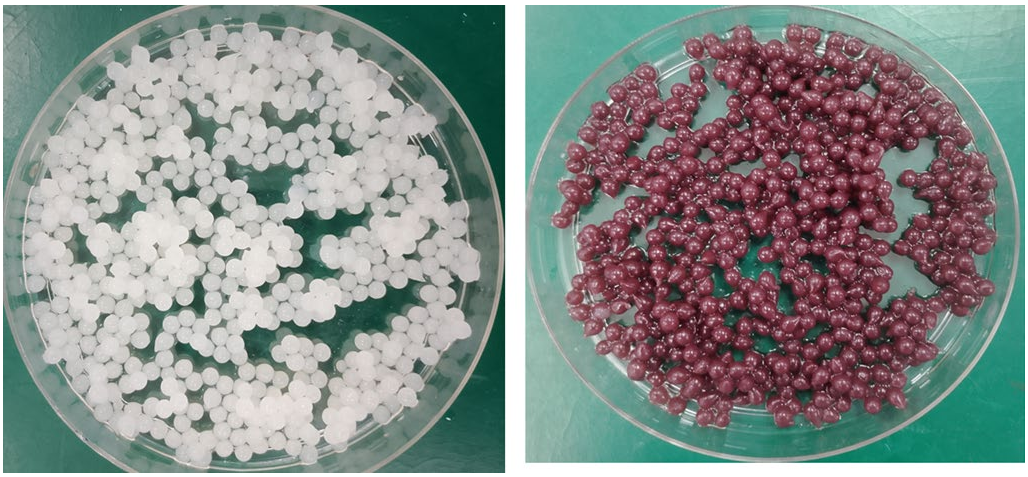

Figure 4. Digital photography of the unmodified and modified calcium alginate beads.

Table 4. Experimental studies in the bubble column bioreactor base on 5g/L of glucose.

Response	Runs			Average	%Error
	1	2	3		
Ethanol Concentration (g/L)	3.75	3.77	3.90	3.8067	2.1
Residual Glucose Conc. (g/L)	0.105	0.104	0.110	0.106	2.32
Ethanol Yield (% v/V)	45	44.5	43.5	44.3	1.5

Among the selected factors, Time (h) exhibits the highest standardized effect, making it the most influential factor in ethanol production. Prolonged fermentation allows microorganisms to metabolize substrates effectively, increasing ethanol yield, but excessive fermentation time can lead to ethanol toxicity and a shift toward by-product formation [62]. Air Flow Rate (L/min) ranks as the second most significant factor, underscoring the role of oxygen transfer in fermentation. Proper aeration enhances yeast metabolism and ethanol production; however, excessive aeration may favor oxidative pathways, reducing ethanol yield [63-65]. Cell Loading (OD600) is the third most impactful factor, as higher microbial biomass ensures an increased fermentation rate, though excessive cell loading can cause nutrient depletion, leading to substrate inhibition and inefficient ethanol conversion [66-67]. Mass of Bead (g), which supports immobilized fermentation, was the fourth most significant factor. A higher bead mass facilitates enhanced cell retention, improving ethanol productivity, but excessive bead concentration can reduce effective mass transfer and create diffusion limitations [68-69].

In contrast, Temperature (°C) and Substrate Concentration (g/L) fall below the t-value threshold, indicating their statistically insignificant effect within the experimental conditions. While temperature is a critical factor in microbial metabolism, its effect in this study suggests that variations within the tested range did not strongly influence ethanol yield. Substrate concentration, which typically correlates with ethanol yield, also showed a lower impact, suggesting that microbial cells were not substrate-limited under the given conditions. pH was the only factor that exhibited a negative effect, indicating that deviations in pH might have led to unfavorable fermentation conditions, potentially inhibiting enzyme activity or microbial viability [70-71]. By selecting the four most significant factors based on statistical thresholds as shown in Figures 6 and 7, the RSM CCD model can be optimized for ethanol yield with reduced experimental complexity while maintaining predictive accuracy.

3.5 Determining CCD Factor Levels (Including Axial Points)

For a Central Composite Design (CCD), the levels are extended beyond the factorial points using axial points (±α) to capture curvature effects. The typical α value for rotatable CCD is 1.414, therefore the axial points are calculated based on the initial range of values from the factorial experimental design done previously. Table 5 shows the estimation of factors for the CDD RSM design calculated based on Equation (39).

3.6 Analysis of Variance (ANOVA) for the Quadratic Model in Ethanol Yield Optimization

The analysis of variance (ANOVA) for the quadratic model evaluating ethanol yield as

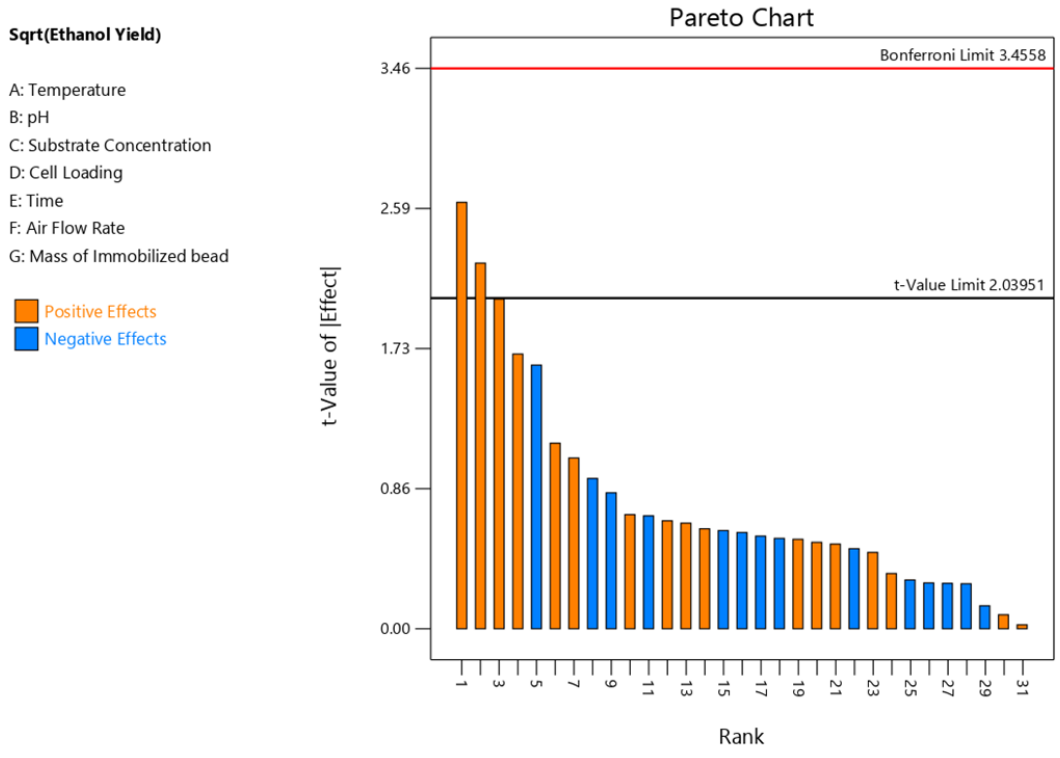

Figure 5. Effect of t-value on the ranking of factors in the Pareto Chart.

shown in Table 6 revealed that the model is statistically significant, with an F-value of 14.14 and a p-value of <0.0001. This confirms that the selected independent variables and their interactions contribute significantly to explaining the variance in ethanol production. Prior studies have similarly emphasized the importance of ANOVA in assessing the reliability of predictive models in bioethanol production, demonstrating its effectiveness in optimizing fermentation conditions [72-73].

Among the individual factors, cell loading (C) exhibited the highest impact on ethanol yield (F = 48.48, p < 0.0001), followed by mass of bead (D) (F = 26.53, p = 0.0001). This aligns with previous research indicating that cell concentration plays a crucial role in fermentation efficiency, affecting both substrate consumption and ethanol productivity [74]. The significant effect of air flow rate (B) (F = 5.88, p = 0.0284) suggests that oxygen availability is a key factor in yeast metabolism, a finding consistent with earlier studies on aerobic fermentation enhancement [74,75]. However, time (A) did not show a significant impact on ethanol yield (p = 0.5013), suggesting that within the studied range, extending the fermentation duration does not necessarily improve ethanol production, which supports findings from previous kinetic modeling studies [74,76].

3.7 Interaction Effects and Quadratic Terms

The study also examined the interactions between factors, revealing that while most interaction terms were not statistically significant, the interaction between cell loading (C) and mass of bead (D) (BD) significantly influenced ethanol yield (F = 18.27, p = 0.0007). This suggests that optimizing the balance between microbial density and bead mass can enhance ethanol productivity, likely due to improved mass transfer and substrate availability, a phenomenon also observed in immobilized yeast systems [78]. Other

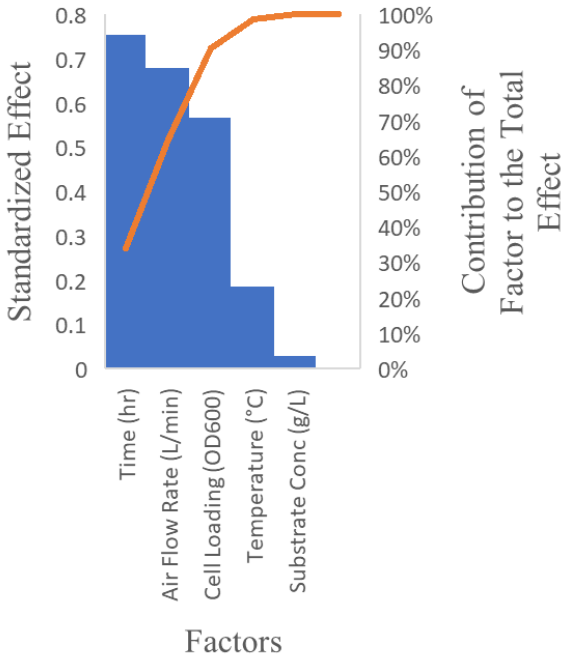

Figure 7. Contribution of each factor to ethanol yield in the factorial design.

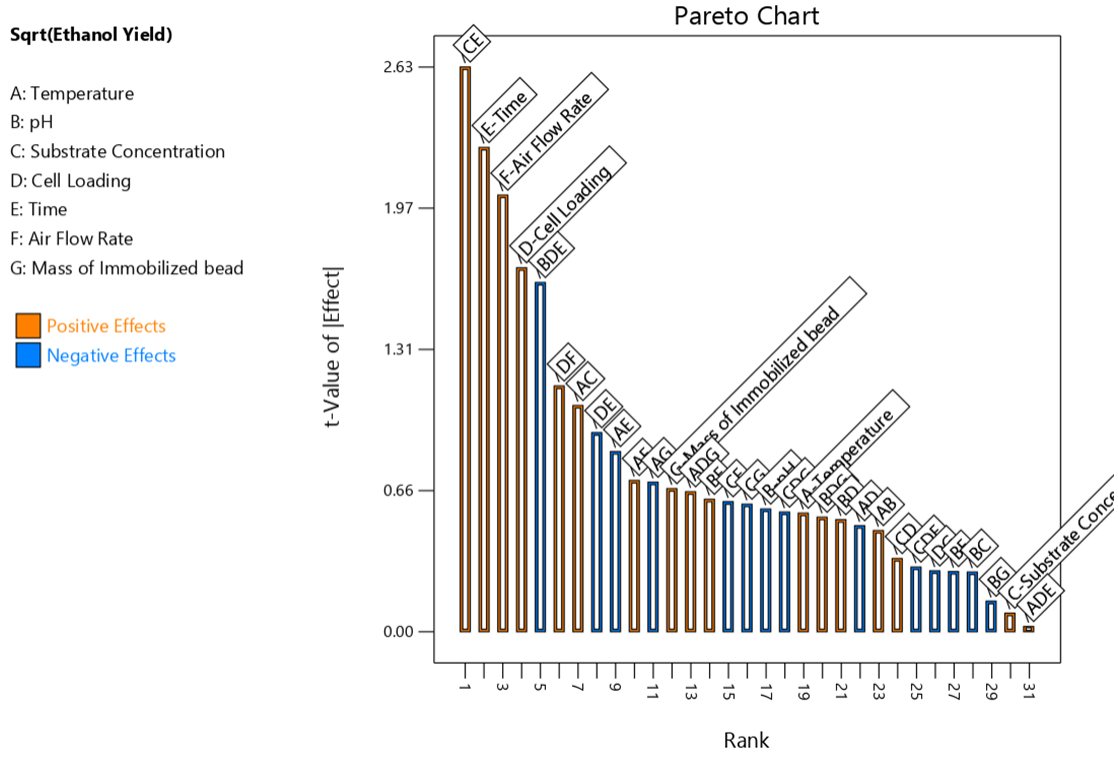

Figure 6. Factor labels on the Pareto chart showing the most significant factors.

interactions, including AB, AC, AD, BC, and CD, were not significant (p-values > 0.1), indicating that their effects on ethanol yield are negligible under the studied conditions.

The quadratic terms demonstrated a substantial impact on ethanol yield, indicating nonlinear relationships between the process variables. The quadratic effects of time (A^2) ($F = 27.31$, $p = 0.0001$), air flow rate (B^2) ($F = 28.81$, $p < 0.0001$), and cell loading (C^2) ($F = 60.80$, $p < 0.0001$) were highly significant, confirming the presence of optimal levels for these variables beyond which ethanol yield declines. Similar findings have been reported in studies applying response surface methodology (RSM) to bioethanol production, where nonlinearity in fermentation parameters necessitated optimization using second-order models [77-79]. The quadratic term for mass of bead (D^2) was also significant ($F = 6.27$, $p = 0.0243$), suggesting that excessive bead mass may hinder yeast mobility, reducing ethanol yield [79].

3.7.1 Model adequacy and lack of fit analysis

The residual error, with a mean square value of 0.1874, was relatively low, indicating good model fit. Furthermore, the lack of fit test ($F = 0.8681$, $p = 0.6046$) was not significant, confirming that the model effectively represents the experimental data without systematic deviations. This is crucial in fermentation process modeling, as inadequate model fitting can lead to erroneous optimization results. The total sum of squares of 39.90 further reinforces that most of the variance in ethanol yield is accounted for by the selected predictors.

3.7.2 Model fit statistics

The model fit statistics as shown in Table 7 confirm the reliability of the regression equation in predicting ethanol yield.

3.7.3 Key statistics

Key statistics include $R^2 = 0.9296$ means strong model fit, explaining 92.96% of variability; Adjusted $R^2 = 0.8638$ means high predictive accuracy, considering model complexity; Predicted $R^2 = 0.7054$ means reasonable predictive capability, though slightly lower; and Adequate Precision = 13.8081 means strong signal-to-noise ratio (>4), confirming model reliability. The final

Table 5. Estimation of factors for the CDD RSM design (negative values of factors were truncated to its minimum feasible value).

Factor	Low (-1)	Center (0)	High (+1)	Axial Low (-α)	Axial High (+α)
Time (h)	24	60	96	11.8	108.2
Air Flow Rate (L/min)	0.5	1.5	2.5	0.07	2.93
Cell Loading (OD600)	1	3	5	0.3	5.7
Mass of Bead (g)	10	30	50	-2.8	62.8

Table 6. ANOVA table for the quadratic model.

Source	Sum of Squares	df	Mean Square	F-value	p-value	Status
Model	37.09	14	2.65	14.14	< 0.0001	significant
A-Time	0.0890	1	0.0890	0.4749	0.5013	
B-Air Flow Rate	1.10	1	1.10	5.88	0.0284	
C-Cell Loading	9.09	1	9.09	48.48	< 0.0001	
D-Mass of Bead	4.97	1	4.97	26.53	0.0001	
AB	0.1314	1	0.1314	0.7015	0.4154	
AC	0.5397	1	0.5397	2.88	0.1103	
AD	0.1987	1	0.1987	1.06	0.3194	
BC	0.0260	1	0.0260	0.1387	0.7148	
BD	3.42	1	3.42	18.27	0.0007	
CD	0.1366	1	0.1366	0.7289	0.4067	
A^2	5.12	1	5.12	27.31	0.0001	
B^2	5.40	1	5.40	28.81	< 0.0001	
C^2	11.39	1	11.39	60.80	< 0.0001	
D^2	1.17	1	1.17	6.27	0.0243	
Residual	2.81	15	0.1874			
Lack of Fit	1.78	10	0.1783	0.8681	0.6046	not significant
Pure Error	1.03	5	0.2055			
Cor Total	39.90	29				

regression model in terms of coded factors is given as shown in Equation (40):

$$Ethanol\ Yield = 46.85 + 0.0609A + 0.2142B + 0.6153C + 0.4551D - 0.0906AB + 0.1837AC + 0.1114AD + 0.0403BC + 0.4625BD + 0.0924CD - 0.4320A^2 - 0.4436B^2 - 0.6445C^2 - 0.2070D^2 \quad (40)$$

The coded equation shows that Cell Loading (C) has the highest positive effect on ethanol yield, followed by Mass of Bead (D). The quadratic terms indicate that the response has an optimal range, beyond which ethanol yield declines.

3.8 Discussion of the Ethanol Contour Plot and Comparison with Literature

The contour plot of ethanol yield (Figure 8) illustrates the relationship between fermentation time and air flow rate, with actual factors C and D held constant. The highest ethanol yield of 47.9% was achieved at around 60 hours of fermentation and an air flow rate of 1.5 L/min. The contour lines suggest that ethanol production is highly sensitive to changes in these variables, as both excessively high and low air flow rates lead to reduced yields. This observation highlights the importance of balancing oxygen availability to optimize yeast metabolism, ensuring sufficient anaerobic conditions without oxygen deprivation. To assess the effectiveness of the optimized conditions in this study, a comparison with previous literature is essential. Several studies have reported lower ethanol yields under different conditions, reinforcing the advantages of the present optimization. For instance, a study by Cheng et al. [80] investigated the effect of air supplementation on continuous ethanol fermentation using *Saccharomyces cerevisiae* STV89. They found that supplying a small amount of oxygen (up to about 80 µmol oxygen/L/h) significantly enhanced ethanol productivity compared to cultures without air supplementation. Specifically, as the air supply rate increased from 0 to 11 mL air/L/h, ethanol yield improved slightly from approximately 37% to 45% of the theoretical maximum. These findings suggest that oxygen supplementation can improve cell viability and ethanol tolerance, leading to enhanced ethanol production.

Table 7. Fit statistics for the quadratic model.

Std. Dev.	0.4329	R^2	0.9296
Mean	45.47	Adjusted R^2	0.8638
C.V. %	0.9520	Predicted R^2	0.7054
		Adeq Precision	13.8081

Similarly, Khongsay *et al.* [81] optimized agitation and aeration conditions for very high gravity ethanol fermentation from sweet sorghum juice using *Saccharomyces cerevisiae* NP 01. The optimal conditions were found to be an agitation rate of 200 rpm, an aeration rate of 2.5 vvm, and an aeration timing of 4 hours. Under these conditions, the ethanol concentration, productivity, and yield were 132.82±1.06 g/L, 2.55±0.00 g/L/h, and 45%, respectively. In contrast, under the same conditions without aeration, ethanol yield was approximately 44%. These results indicate that appropriate aeration and agitation strategies can significantly improve ethanol production under very high gravity conditions. Compared to this study's optimized conditions, it is evident that a moderate aeration strategy enhances ethanol yield, preventing the inefficiencies observed in the aforementioned studies.

3.9 Effects of Process Variables on Ethanol Yield in a Bubble Column Bioreactor

The six 3D response surface plots as shown in Figure 9 reveal key interactions between process variables affecting ethanol yield in the bubble column bioreactor. Symmetry is observed in some plots, such as Mass of Bead & Cell Loading and Cell Loading & Time, suggesting stable and predictable relationships where an optimal balance enhances ethanol production. However, asymmetry is evident in plots like Air Flow Rate & Time and Mass of Bead & Air Flow Rate, indicating potential limitations such as oxygen transfer constraints or substrate depletion at extreme conditions.

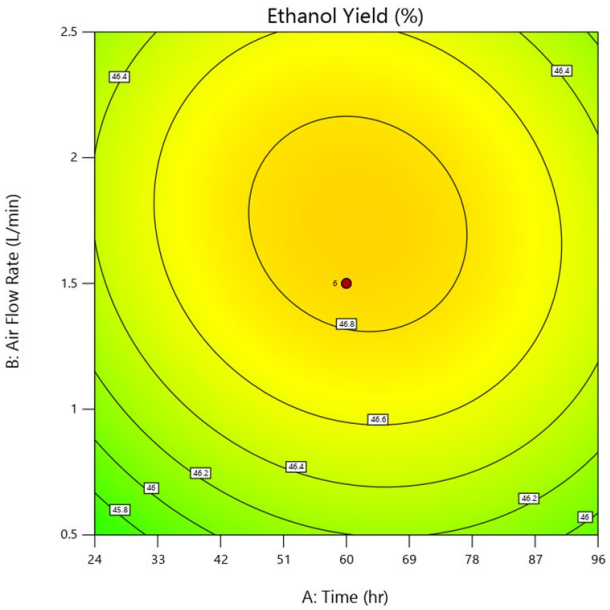

Figure 8. Contour plot of ethanol yield as a function of fermentation time and air flow rate.

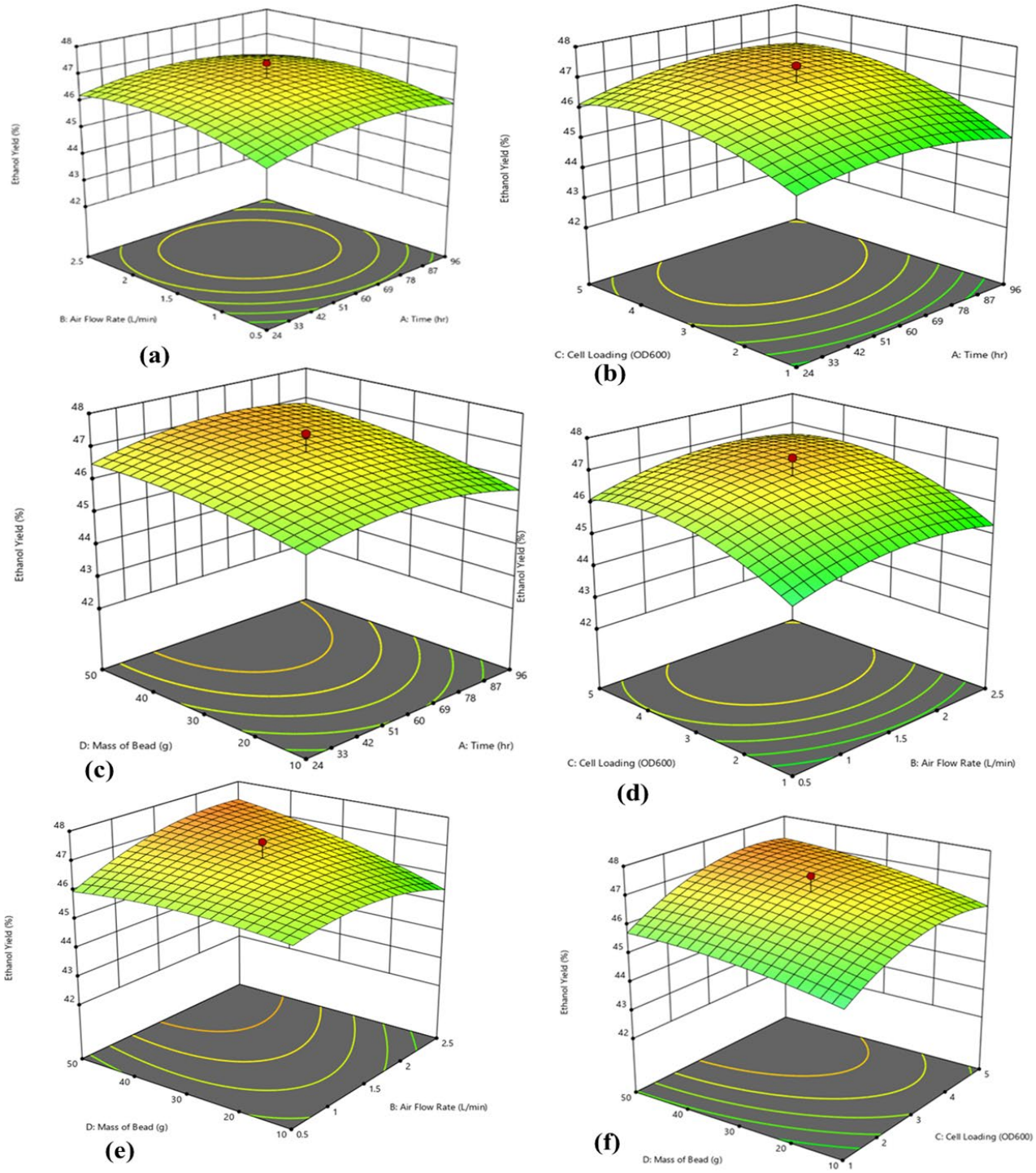

Figure 9. (a) The interaction between Air flow rate and Time, (b) Interaction between Cell loading and Time, (c)Interaction between mass of bead and Time, (d) The interaction between Cell Loading and Air flow rate, (e) The Interaction between Mass of beads and Air flow rate (f) The interaction between beads mass and Cell Loading.

Response sensitivity varies across the plots; for instance, steep slopes in Cell Loading & Air Flow Rate highlight their strong influence on ethanol yield, whereas flatter areas in Mass of Bead & Time suggest a saturation point beyond which further increases have minimal impact. These findings emphasize the importance of optimizing key variables to maintain stability while preventing inefficiencies caused by excessive aeration or cell loading. The findings from the 3D plots indicate that ethanol yield in a bubble column bioreactor is highly dependent on the interplay between mass of beads, cell loading, air flow rate, and fermentation time. Identifying optimal conditions for these variables is critical to enhancing fermentation efficiency. Future studies could focus on refining these parameters through advanced modeling approaches and experimental validation to achieve consistent and high ethanol yields [82-86].

3.10 Validation Results

The validation experiment was conducted under the optimized conditions of 60 hours of fermentation time and an air flow rate of 1.5 L/min. The experimental ethanol yield values were 47.5%, 47.6%, and 47.4%, closely matching the model's predicted yield of 47.9%. The percentage error as shown in Table 8, calculated as the deviation from the predicted value, ranged between 0.63% and 1.04%, with an average error of 0.84%, indicating high accuracy of the model.

These results confirm the robustness and reliability of the developed model in predicting ethanol yield under optimized conditions. The minimal deviation suggests that the experimental setup effectively replicated the optimized parameters, supporting the practical applicability of the findings for industrial bioethanol production.

4. Conclusion

This study successfully demonstrated the computational modeling, process optimization, and validation of a laboratory-scale bubble column bioreactor (BCB) for bioethanol fermentation. The Python-based simulations provided detailed insights into oxygen transfer dynamics, glucose consumption kinetics, biomass growth, and ethanol production, allowing for precise parameter optimization. The incorporation of dynamic aeration control, pH stabilization, temperature regulation, and foam suppression algorithms ensured a well-regulated fermentation environment. The results confirmed that a working volume of 500 mL, an oxygen uptake rate (*OUR*) of 1.1 g O_2/g cells, a volumetric oxygen transfer coefficient (k_La) of 50 h^{-1}, and a glucose consumption rate of 2 g/L·h were optimal for efficient ethanol synthesis, maintaining process stability and scalability. The performance test revealed an ethanol yield of 44.3%, demonstrating the efficiency of the fermentation process under the given operational conditions. This yield suggests a moderate conversion of glucose to ethanol, which may be influenced by factors such as substrate concentration, aeration rate, temperature control, and microbial activity. Further optimization of these parameters could potentially enhance ethanol production. Additionally, the yield aligns with previously reported values in similar bioreactor configurations, indicating the reliability of the experimental setup.

Abbreviations

F_{O_2} = Oxygen flow rate (m^3/s or L/min)
$C_{O_2,in}$ = Oxygen concentration in the inlet gas (g O_2 /L)
k_La = Volumetric mass transfer coefficient (1/h)
V = Reactor volume (L or m^3)
C_{O_2*} = Saturation oxygen concentration (g O_2/L)
C_{O_2} = Dissolved oxygen concentration (g O_2/L)
rO_2 = Oxygen uptake rate (OUR) (g O_2/L · h)
$X(t)$ = Biomass concentration at time **t** (g/L)
X_o = Initial biomass concentration (0.1 g /L, assumed)
μ = Specific growth rate (0.3 h^{-1}, assumed)
t = Time (h)
k_{CO_2} = 0.05 (empirical factor linking CO_2 to pH drop)
pH_o = 5.5 (initial pH)
$Y_{O_2/X}$ = Oxygen yield coefficient on biomass (g O_2 /g cells)
$Y_{X/S}$ = Biomass yield on glucose (g cells/g glucose)
r_S = Glucose consumption rate (g glucose/L · h)
P_{O_2} = Partial pressure of oxygen in bubbles (atm)
H = Henry's constant for oxygen solubility (atm · L/mol)
V_L = Liquid volume (excluding bubbles)
F_{O_2} = Oxygen flow rate (m^3/s)

Table 8. Validation of ethanol yield under optimized conditions.

Run	Time (h)	Air Flow Rate (L/min)	Predicted Yield (%)	Experimental Yield (%)	Error (%)
1	60	1.5	47.9	47.5	0.84
2	60	1.5	47.9	47.6	0.63
3	60	1.5	47.9	47.4	1.04
Average	60	1.5	47.9	47.5	0.84

ρ_g = Density of air (1.225 kg/m^3 at 25°C)
H_t
= Height of the liquid column (m) (assumed 0.3 m)
η = Aeration efficiency (typically 50%)
g = Gravitational acceleration (9.81 m/s^2)
$S\ (t)$ = Glucose concentration at time **t** (g/L)
S_o = Initial glucose concentration (50 g/L)
r_s = Glucose consumption rate (2 g/L · h)

Acknowledgment

This research was funded by Petronas Malaysia under grant number UIC240814. The authors acknowledge Federal University Wukari for institutional support and resources provided for this research.

CRedit Author Statement

Author Contributions: David Abutu (DA): Conceptualized the study and designed the bioreactor; Hafizuddin Wan Yussof (HWY): Performed computational simulations and optimization; Benjamin Aderemi (BA): Contributed to data analysis and manuscript writing; Ameh Alewo Opueda (AAO): Assisted in computational modeling and interpretation of results; Augustine Agi (AA): Provided critical revisions and technical insights. All authors have read and agreed to the published version of the manuscript.

Availability of Data and Materials

The datasets used and analyzed during this study are provided in the supplementary information file attached.

References

[1] Abdul Kareem Joyia, M., Ahmad, M., Chen, Y.-F., Mustaqeem, M., Ali, A., Abbas, A., Ashraf Gondal, M. (2024) Trends and advances in sustainable bioethanol production technologies from first to fourth generation: A critical review, *Energy Conversion and Management*, 321, 119037. DOI: 10.1016/j.enconman.2024.119037.

[2] Mohd Azhar, S.H., Abdulla, R., Jambo, S.A., Marbawi, H., Gansau, J.A., Mohd Faik, A.A., Rodrigues, K.F. (2017). Yeasts in sustainable bioethanol production: A review, *Biochem. Biophys. Rep.*, 10, 52–61. DOI: 10.1016/j.bbrep.2017.03.003.

[3] Mustafa, G., Alvi, A., Batool, S.T., Ilyas, H., Zahid, M.T., Jeon, B.-H., Shafiq, Z., Abbas, S.Z., Anwar, N., Rafatullah, M. (2025). Design of the novel bioreactors for efficient bioconversion of lignocellulose into bioethanol, in *Biofuels and Sustainability*, (pp. 395–421). Elsevier. DOI: 10.1016/B978-0-443-21433-2.00021-9.

[4] Mutaf, T., Oncel, S.S. (2023) Bubble column and airlift bioreactor systems for animal cell culture applications, *Asia-Pacific Journal of Chemical Engineering*, 18(1). DOI: 10.1002/apj.2872.

[5] de Jesus, S.S., Moreira Neto, J., Maciel Filho, R. (2017). Hydrodynamics and mass transfer in bubble column, conventional airlift, stirred airlift and stirred tank bioreactors, using viscous fluid: A comparative study, *Biochem. Eng. J.*, 118, 70–81, DOI: 10.1016/j.bej.2016.11.019.

[6] Abutu, D., Aderemi, B.O., Ameh, A.O., Yussof, H.W., Agi, A. (2025). Nano-enhanced biocarriers: ferric oxide-modified chitosan and calcium alginate beads for improved fermentation efficiency and reusability in a bubble column bioreactor, *Biotechnol. Lett.*, 47(4), 70, DOI: 10.1007/s10529-025-03611-6.

[7] Thanapornsin, T., Sirisantimethakom, L., Laopaiboon, L., Laopaiboon, P. (2022). Effectiveness of Low-Cost Bioreactors Integrated with a Gas Stripping System for Butanol Fermentation from Sugarcane Molasses by Clostridium beijerinckii, *Fermentation*, 8(5), 214, DOI: 10.3390/fermentation8050214.

[8] Yerima, E.A., Maaji, S.P., Samuel-Okey, F.C., Abutu, D., Afyenaku, S., Mudwa, D., Audu, S. (2025) An efficient and optimal adsorptive removal of glufosinate ammonium from wastewater using carbonized rice husk-clay blend briquettes, *Ecological Engineering & Environmental Technology*, 26(9), 1–12, DOI: 10.12912/27197050/208147.

[9] Abutu, D., Aderemi, B.O., Ameh, A.O., Yussof, H.W., Gbonhinbor, J., Money, B., Nyah, F., Umunnawuike, C., Nwaichi, P.I., Agi, A. (2025) Optimization of Ethanol Fermentation in a Bubble Column Bioreactor Using Response Surface Methodology with Ferric Oxide Nanoparticle-Modified Supports, *SPE Nigeria Annual International Conference and Exhibition*, SPE, DOI: 10.2118/228638-MS.

[10] Mast, Y., Ghaderi, A., Takors, R. (2025) Real Case Study of 600 m3 Bubble Column Fermentations: Spatially Resolved Simulations Unveil Optimization Potentials for l-Phenylalanine Production With *Escherichia coli*, *Biotechnol. Bioeng.*, 122(2), 265–286, DOI: 10.1002/bit.28869.

[11] MÃller, K., Bro, C., PiÅkur, J., Nielsen, J., Olsson, L. (2002) Steady-state and transient-state analyses of aerobic fermentation in *Saccharomyces kluyveri*, *FEMS Yeast Res.*, 2(2), 233–244, DOI: 10.1111/j.1567-1364.2002.tb00088.x.

[12] Visser, W., Scheffers, W.A., Batenburg-van der Vegte, W.H., van Dijken, J.P. (1990) Oxygen requirements of yeasts, *Appl. Environ. Microbiol.*, 56(12), 3785–3792, DOI: 10.1128/aem.56.12.3785-3792.1990.

[13] Karadag, D., Puhakka, J.A. (2010) Direction of glucose fermentation towards hydrogen or ethanol production through on-line pH control, *Int. J. Hydrogen Energy*, 35(19), 10245–10251, DOI: 10.1016/j.ijhydene.2010.07.139.

[14] Coletto, A., Poesio, P. (2024) Hold-up formation in bubble channel reactors: A bubble-scale investigation, *Chemical Engineering Research and Design*, 201, 1–17, DOI: 10.1016/j.cherd.2023.11.028.

[15] Du, Y., Li, Y., Ren, P., Zhang, L., Wang, D., Xu, X. (2024) Oxygen transfer at mesoscale catalyst layer in proton exchange membrane fuel cell: Mechanism, model and resistance characterization, *Chemical Engineering Journal*, 494, 153021, DOI: 10.1016/j.cej.2024.153021.

[16] Silva, C.A.A., Fonseca, G.G. (2024) Physiological parameters as a key tool for understanding and optimizing yeast metabolism and physiology in batch cultures, *Chem. Eng. Commun.*, 211(12), 1908–1920, DOI: 10.1080/00986445.2024.2386310.

[17] Yalçin, S.K., Özbas, Z.Y. (2004) Effects of different substrates on growth and glycerol production kinetics of a wine yeast strain Saccharomyces cerevisiae Narince 3, *Process Biochemistry*, 39(10), 1285–1291, DOI: 10.1016/S0032-9592(03)00252-8.

[18] van Zyl, W.H., Lynd, L.R., den Haan, R., McBride, J.E. (2007) Consolidated Bioprocessing for Bioethanol Production Using Saccharomyces cerevisiae, 205–235. DOI: 10.1007/10_2007_061.

[19] Wu, W.-H., Hung, W.-C., Lo, K.-Y., Chen, Y.-H., Wan, H.-P., Cheng, K.-C. (2016) Bioethanol production from taro waste using thermo-tolerant yeast Kluyveromyces marxianus K21, *Bioresour. Technol.*, 201, 27–32, DOI: 10.1016/j.biortech.2015.11.015.

[20] Turbin-Orger, A., Babin, P., Boller, E., Chaunier, L., Chiron, H., Della Valle, G., Dendievel, R., Réguerre, A.L., Salvo, L. (2015) Growth and setting of gas bubbles in a viscoelastic matrix imaged by X-ray microtomography: the evolution of cellular structures in fermenting wheat flour dough, *Soft Matter.*, 11(17), 3373–3384, DOI: 10.1039/C5SM00100E.

[21] Dong, L., Wang, W., Xie, Q., Du, X., Wang, Y., Niu, X.-Z., Cao, G. (2025) Self-adaptable HAc/NaAc buffer system enhanced biohydrogen production from dark fermentation of cellulose, *Bioresour. Technol.*, 416, 131738, DOI: 10.1016/j.biortech.2024.131738.

[22] Jia, M., Zhu, Y., Wang, L., Sun, T., Pan, H., Li, H. (2022) pH Auto-Sustain-Based Fermentation Supports Efficient Gamma-Aminobutyric Acid Production by Lactobacillus brevis CD0817, *Fermentation*, 8(5), 208, DOI: 10.3390/fermentation8050208.

[23] Easwaran, S., Subramanian, A.M., Aadimoolam, S., Surianarayanan, M. (2024) Metabolic heat response of Kluyveromyces marxianus during Carboxypeptidase Y Production; Effect of Agitation, Aeration and pH control, *Process Biochemistry*, 112, 71-79. DOI: 10.22541/au.170667299.96643066/v1.

[24] Junker, B. (2007) Foam and Its Mitigation in Fermentation Systems, *Biotechnol. Prog.*, 23(4), 767–784, DOI: 10.1021/bp070032r.

[25] Damayanti, A., Bahlawan, Z.A.S., Kumoro, A.C. (2022) Modeling of bioethanol production through glucose fermentation using Saccharomyces cerevisiae immobilized on sodium alginate beads, *Cogent Eng.*, 9(1), DOI: 10.1080/23311916.2022.2049438.

[26] Novia, N., Hasanudin, H., Hermansyah, H., Fudholi, A., Pareek, V.K. (2023) Recent advances in CFD modeling of bioethanol production processes, *Renewable and Sustainable Energy Reviews*, 183, 113522, DOI: 10.1016/j.rser.2023.113522.

[27] Nyah, F., Ridzuan, N., Epelle, E., Abd Aziz, M.A.B., Money, B., Abutu, D., Agi, A. (2025) Cellulose bionanomaterial design for enhanced oil recovery: A review of existing, emerging technologies and future outlook, *Petroleum Research*, DOI: 10.1016/j.ptlrs.2025.12.002.

[28] Yerima, E.A., Maaji, S.P., Ogbodo, C.V., Abutu, D., Yakubu, S.A., Nwankwo, F.O., Adamu, J.A. (2026) Efficient and optimal adsorptive removal of urea from agricultural effluent using acidified ball clay: optimization via response surface methodology, *African Scientific Reports*, 367, DOI: 10.46481/asr.2026.5.1.367.

[29] Wang, Y., Chan, K.-L., Abdel-Rahman, M. A., Sonomoto, K., Leu, S.-Y. (2020) Dynamic simulation of continuous mixed sugar fermentation with increasing cell retention time for lactic acid production using Enterococcus mundtii QU 25, *Biotechnol. Biofuels*, 13(1), 112, DOI: 10.1186/s13068-020-01752-6.

[30] González-Gloria, K.D., Rodríguez-Jasso, R.M., Saxena, R., Sindhu, R., Ali, S.S., Singhania, R.R., Ruiz, H.A. (2022) Bubble column bioreactor design and evaluation for bioethanol production using simultaneous saccharification and fermentation strategy from hydrothermally pretreated lignocellulosic biomass, *Biochem. Eng. J.*, 187, 108645, DOI: 10.1016/j.bej.2022.108645.

[31] Taghizadeh, M.H., Khajeh, K., Nasirpour, N., Mousavi, S.M. (2024) Maximization of uricase production in a column bioreactor through response surface methodology-based optimization, *Biofabrication*, 16(3), 035023, DOI: 10.1088/1758-5090/ad467f.

[32] Mast, Y., Ghaderi, A., Takors, R. (2025) Real Case Study of 600 m^3 Bubble Column Fermentations: Spatially Resolved Simulations Unveil Optimization Potentials for l-Phenylalanine Production With *Escherichia coli*, *Biotechnol. Bioeng.*, 122(2), 265–286, DOI: 10.1002/bit.28869.

[33] Almeida Benalcázar, E., Noorman, H., Maciel Filho, R., Posada, J.A. (2020) Modeling ethanol production through gas fermentation: a biothermodynamics and mass transfer-based hybrid model for microbial growth in a large-scale bubble column bioreactor, *Biotechnol. Biofuels*, 13(1), 59, DOI: 10.1186/s13068-020-01695-y.

[34] Abutu, D., Nwaichi, P.I., Umunnawuike, C., Nyah, F., Money, B., Yussof, H.W., Agi, A. (2025) Numerical Simulation of Microbial Biohydrogen Production under High-Pressure, High-Temperature Conditions for Enhanced Recovery from Depleted Reservoirs, *Petroleum Research*, DOI: 10.1016/j.ptlrs.2025.07.006.

[35] David, A., Aderemi, B., Ameh, A.O. (2025) Development and Construction of a Laboratory-Scale Bubble Column Bioreactor for Immobilized Enzyme Fermentation Studies, in *The 3rd International Electronic Conference on Catalysis Sciences: Session Catalytic Materials*, Narendra Kumar, Ed., Basel, Switzerland: MDPI, Apr. 2025.

[36] Umunnawuike, C., Abutu, D., Nwaichi, P.I., Nyah, F., Agi, A. (2026) Optimizing thermophilic fermentation for hydrogen production in depleted oil reservoirs, *J. Environ. Chem. Eng.*, 14(1), 121160, DOI: 10.1016/j.jece.2026.121160.

[37] Umunnawuike, C., Abutu, D., Nwaichi, P.I., Nyah, F., Agi, A. (2026) Thermophilic biohydrogen production from reservoir residual hydrocarbons using palm oil mill effluent–derived microbial consortia, *Science of The Total Environment*, 1016, 181482, DOI: 10.1016/j.scitotenv.2026.181482.

[38] Money, B., Mahat, S.Q.A.B., Ismail, N., Modather, R.H., David, A., Nyah, F., ... & Agi, A. (2025) Characterization of Kuala Rompin clay (KRC) and empty fruit bunch ash (EFBA) for potential application in the formulation of geopolymer cement, *Discover Concrete and Cement*, 1(1), 12, DOI: 10.1007/s44416-025-00012-w.

[39] Abutu, D., Ameh, A.O., Umunnawuike, C., Barima, M., Nyah, F., Nwaichi, P.I., ... & Yerima, E.A. (2025) Reinforcing concrete with nano-enhanced bio-additives: a path toward sustainable construction materials, *Discover Concrete and Cement*, 1(1), 20, DOI: 10.1007/s44416-025-00022-8.

[40] Abutu, D., Wan Yussof, H., Nyah, F., Ikechukwu Nwaichi, P., Umunnawuike, C., Agi, A. (2026) Modelling biohydrogen production from residual hydrocarbons by immobilized bacteria using COMSOL multiphysics, *Biomass Bioenergy*, 211, 109165, DOI: 10.1016/j.biombioe.2026.109165.

[41] Li, X., Lu, Y., Luo, H., Liu, G., Torres, C.I., Zhang, R. (2021) Effect of pH on bacterial distributions within cathodic biofilm of the microbial fuel cell with maltodextrin as the substrate, *Chemosphere*, 265, 129088, DOI: 10.1016/j.chemosphere.2020.129088.

[42] Alam, M.A., Yuan, T., Xiong, W., Zhang, B., Lv, Y., Xu, J. (2019) Process optimization for the production of high-concentration ethanol with Scenedesmus raciborskii biomass, *Bioresour. Technol.*, 294, 122219, DOI: 10.1016/j.biortech.2019.122219.

[43] Agbor, E.A., Tiku, P.B., Hermann, M.D. (2022) Effect of Microbial Inoculant on Physicochemical and Microbiological Properties of Cassava Fermentation Process and Fufu Produced, *Asian Food Science Journal*, 21(3), 1-9. DOI: 10.9734/afsj/2022/v21i330411.

[44] Bonan, C.I., Biazi, L.E., Dionísio, S.R., Soares, L.B., Tramontina, R., Sousa, A.S., Ienczak, J.L. (2020) Redox potential as a key parameter for monitoring and optimization of xylose fermentation with yeast Spathaspora passalidarum under limited-oxygen conditions, *Bioprocess Biosyst. Eng.*, 43(8), 1509–1519, DOI: 10.1007/s00449-020-02344-2.

[45] Bonan, C.I.D.G., Tramontina, R., dos Santos, M.W., Biazi, L.E., Soares, L.B., Pereira, I.O., Hoffmam, Z.B., Coutouné, N., Squina, F.M., Robl, D., Ienczak, J.L. (2022) Biorefinery Platform for Spathaspora passalidarum NRRL Y-27907 in the Production of Ethanol, Xylitol, and Single Cell Protein from Sugarcane Bagasse. *Bioenerg. Res.* 15, 1169–1181. DOI: 10.1007/s12155-021-10255-7.

[46] Shin, W.-S., (2013) Application of Scale-Up Criterion of Constant Oxygen Mass Transfer Coefficient (kLa) for Production of Itaconic Acid in a 50 L Pilot-Scale Fermentor by Fungal Cells of Aspergillus terreus, *J. Microbiol. Biotechnol.*, 23(10), 1445–1453, DOI: 10.4014/jmb.1307.07084.

[47] Esperança, M.N., Mendes, C.E., Rodriguez, G.Y., Cerri, M.O., Béttega, R., Badino, A.C. (2020) Sparger design as key parameter to define shear conditions in pneumatic bioreactors, *Biochem. Eng. J.*, 157, 107529, DOI: 10.1016/j.bej.2020.107529.

[48] Wei, C., Wu, B., Li, G., Chen, K., Jiang, M., Ouyang, P. (2014) Comparison of the hydrodynamics and mass transfer characteristics in internal-loop airlift bioreactors utilizing either a novel membrane-tube sparger or perforated plate sparger, *Bioprocess Biosyst. Eng.*, 37(11), 2289–2304, DOI: 10.1007/s00449-014-1207-4.

[49] Chaudhary, G., Luo, R., George, M., Tescione, L., Khetan, A., Lin, H. (2020) Understanding the effect of high gas entrance velocity on Chinese hamster ovary (CHO) cell culture performance and its implications on bioreactor scale-up and sparger design, *Biotechnol. Bioeng.*, 117(6), 1684–1695, DOI: 10.1002/bit.27314.

[50] Elmisaoui, S., Elmisaoui, S., Benjelloun, S., Khamar, L., Khamar, M. (2022) CFD Investigation of Industrial Gas-Liquid Preneutralizer Based on a Bioreactor Benchmark for Spargers Optimization, *Chem. Eng. Trans.*, 93, 73–78, DOI: 10.3303/CET2293013.

[51] Zu, L., Zhou, H., Yang, S., Li, X., Yang, C., Mao, Z.-S. (2015) Configuration Optimization and Mass Transfer in a Dual-Impeller Bioreactor, *Journal of Chemical Engineering of Japan*, 48(5), 360–366, DOI: 10.1252/jcej.14we018.

[52] Pino, M.S., Rodríguez-Jasso, R.M., Michelin, M., Flores-Gallegos, A.C., Morales-Rodriguez, R., Teixeira, J.A., Ruiz, H.A. (2018). Bioreactor design for enzymatic hydrolysis of biomass under the biorefinery concept, *Chemical Engineering Journal*, 347, 119–136, DOI: 10.1016/j.cej.2018.04.057.

[53] Sonego, J.L.S., Lemos, D.A., Pinto, C.E.M., Cruz, A.J.G., Badino, A.C. (2016) Extractive Fed-Batch Ethanol Fermentation with CO_2 Stripping in a Bubble Column Bioreactor: Experiment and Modeling, *Energy & Fuels*, 30(1), 748–757, DOI: 10.1021/acs.energyfuels.5b02320.

[54] Roy, P., Dutta, A., Chang, S. (2016) Development and evaluation of a functional bioreactor for CO fermentation into ethanol, *Bioresour. Bioprocess.*, 3(1), 4, DOI: 10.1186/s40643-016-0082-z.

[55] Sonego, J.L.S., Lemos, D.A., Pinto, C.E.M., Cruz, A.J.G., Badino, A.C. (2016) Extractive Fed-Batch Ethanol Fermentation with CO_2 Stripping in a Bubble Column Bioreactor: Experiment and Modeling, *Energy & Fuels*, 30(1), 748–757, DOI: 10.1021/acs.energyfuels.5b02320.

[56] de Medeiros, E.M., Posada, J.A., Noorman, H., Filhob, R.M. (2019) Modeling and Multi-Objective Optimization of Syngas Fermentation in a Bubble Column Reactor, In *Computer Aided Chemical Engineering* (Vol. 46, pp. 1531-1536). Elsevier. DOI: 10.1016/B978-0-12-818634-3.50256-3.

[57] Garcia-Ochoa, F., Gomez, E., Santos, V.E., Merchuk, J.C. (2010) Oxygen uptake rate in microbial processes: An overview, *Biochem. Eng. J.*, 49(3), 289–307, DOI: 10.1016/j.bej.2010.01.011.

[58] Laplace, J.M., Delgenes, J.P., Moletta, R., Navarro, J.M. (1991) Alcoholic fermentation of glucose and xylose by Pichia stipitis, Candida shehatae, Saccharomyces cerevisiae and Zymomonas mobilis: oxygen requirement as a key factor, *Appl. Microbiol. Biotechnol.*, 36(2), 158–162, DOI: 10.1007/BF00164412.

[59] Zhang, Z., Xiong, F., Wang, Y., Dai, C., Xing, Z., Dabbour, M., Mintah, B., He, R., Ma, H. (2019) Fermentation of Saccharomyces cerevisiae in a one liter flask coupled with an external circulation ultrasonic irradiation slot: Influence of ultrasonic mode and frequency on the bacterial growth and metabolism yield, *Ultrason. Sonochem.*, 54, 39–47, DOI: 10.1016/j.ultsonch.2019.02.017.

[60] González-Gloria, K.D., Rodríguez-Jasso, R.M., Saxena, R., Sindhu, R., Ali, S.S., Singhania, R.R. (2022) Bubble column bioreactor design and evaluation for bioethanol production using simultaneous saccharification and fermentation strategy from hydrothermally pretreated lignocellulosic biomass, *Biochem. Eng. J.*, 187, 108645, DOI: 10.1016/j.bej.2022.108645.

[61] Sriputorn, B., Laopaiboon, P., Phukoetphim, N., Uppatcha, N., Phuphalai, W., Laopaiboon, L. (2021) Very high gravity ethanol fermentation from sweet sorghum stem juice using a stirred tank bioreactor coupled with a column bioreactor, *J. Biotechnol.*, 332, 1–10, DOI: 10.1016/j.jbiotec.2021.03.012.

[62] Abbaspour, N. (2024) Fermentation's pivotal role in shaping the future of plant-based foods: An integrative review of fermentation processes and their impact on sensory and health benefits, *Applied Food Research*, 4(2), 100468, DOI: 10.1016/j.afres.2024.100468.

[63] Joyia, M.A.K., Ahmad, M., Chen, Y.F., Mustaqeem, M., Ali, A., Abbas, A., Gondal, M.A. (2024) Trends and advances in sustainable bioethanol production technologies from first to fourth generation: A critical review, *Energy Convers. Manag.*, 321, 119037, DOI: 10.1016/j.enconman.2024.119037.

[64] Jain, S., Kumar, S. (2024) A comprehensive review of bioethanol production from diverse feedstocks: Current advancements and economic perspectives, *Energy*, 296, 131130, DOI: 10.1016/j.energy.2024.131130.

[65] Baeyens, J., Kang, Q., Appels, L., Dewil, R., Lv, Y., Tan, T. (2015) Challenges and opportunities in improving the production of bio-ethanol," *Prog. Energy Combust. Sci.*, 47, 60–88, DOI: 10.1016/j.pecs.2014.10.003.

[66] Deshavath, N.N., Woodruff, W., Singh, V. (2024) Sustainable strategies to achieve industrial ethanol titers from different bioenergy feedstocks: scale-up approach for better ethanol yield, *Sustain. Energy Fuels*, 8(15), 3386–3398, DOI: 10.1039/D4SE00520A.

[67] Song, G., Sun, C., Madadi, M., Dou, S., Yan, J., Huan, H., Ashori, A. (2024) Dual assistance of surfactants in glycerol organosolv pretreatment and enzymatic hydrolysis of lignocellulosic biomass for bioethanol production, *Bioresour. Technol.*, 395, 130358, DOI: 10.1016/j.biortech.2024.130358.

[68] Najim, A.A., Radeef, A.Y., al-Doori, I., Jabbar, Z.H., (2024) Immobilization: the promising technique to protect and increase the efficiency of microorganisms to remove contaminants, *Journal of Chemical Technology & Biotechnology*, 99(8), 1707–1733, DOI: 10.1002/jctb.7638.

[69] Liu, Y., Zhang, G., Li, Y., Wu, X., Shang, S., Che, W. (2024) Enhancing immobilized Chlorella vulgaris growth with novel buoyant barium alginate bubble beads, *Bioresour. Technol.*, 406, 130996, DOI: 10.1016/j.biortech.2024.130996.

[70] Qin, Y., Zhai, C., (2024) Global Stabilizing Control of a Continuous Ethanol Fermentation Process Starting from Batch Mode Production, *Processes*, 12(4), 819, DOI: 10.3390/pr12040819.

[71] Akroum, H., Akroum-Amrouche, D., Aibeche, A. (2024) Modeling of conversion kinetics in bioenergy production technologies, *Int. J. Green Energy*, 21(15), 3415–3430, DOI: 10.1080/15435075.2024.2377355.

[72] Manmai, N., Unpaprom, Y., Ponnusamy, V.K., Ramaraj, R. (2020) Bioethanol production from the comparison between optimization of sorghum stalk and sugarcane leaf for sugar production by chemical pretreatment and enzymatic degradation, *Fuel*, 278, 118262, DOI: 10.1016/j.fuel.2020.118262.

[73] Abbaspour, N. (2024) Fermentation's pivotal role in shaping the future of plant-based foods: An integrative review of fermentation processes and their impact on sensory and health benefits, *Applied Food Research*, 4(2), 100468, DOI: 10.1016/j.afres.2024.100468.

[74] Duncan, J.D., Devillers, H., Camarasa, C., Setati, M.E., Divol, B. (2024) Oxygen alters redox cofactor dynamics and induces metabolic shifts in Saccharomyces cerevisiae during alcoholic fermentation, *Food Microbiol.*, 124, 104624, DOI: 10.1016/j.fm.2024.104624.

[75] Bisschops, M., Vos, T., Martinez-Moreno, R., de la Torre Cortes, P., Pronk, J., Daran-Lapujade, P. (2015) Oxygen availability strongly affects chronological lifespan and thermotolerance in batch cultures of Saccharomyces cerevisiae, *Microbial Cell*, 2(11), 429–444, DOI: 10.15698/mic2015.11.238.

[76] Sulieman, A.K., Putra, M.D., Abasaeed, A.E., Gaily, M.H., Al-Zahrani, S.M., Zeinelabdeen, M.A. (2018) Kinetic modeling of the simultaneous production of ethanol and fructose by Saccharomyces cerevisiae, *Electronic Journal of Biotechnology*, 34, 1–8, DOI: 10.1016/j.ejbt.2018.04.006.

[77] Zani, S.H.M., Asri, F.M., Azmi, N.S., Yussof, H.W., Zahari, M.A.K.M. (2019) Optimization of process parameters for bioethanol production from oil palm frond juice by Saccharomyces cerevisiae using response surface methodology as a tool, *IOP Conf. Ser. Mater. Sci. Eng.*, 702(1), 012003, DOI: 10.1088/1757-899X/702/1/012003.

[78] Pereira, L.M.S., Milan, T.M., Tapia-Blácido, D.R. (2021) Using Response Surface Methodology (RSM) to optimize 2G bioethanol production: A review, *Biomass Bioenergy*, 151, 106166, DOI: 10.1016/j.biombioe.2021.106166.

[79] Veza, I., Spraggon, M., Fattah, I.M.R., Idris, M. (2023) Response surface methodology (RSM) for optimizing engine performance and emissions fueled with biofuel: Review of RSM for sustainability energy transition, *Results in Engineering*, 18, 101213, DOI: 10.1016/j.rineng.2023.101213.

[80] Chang, Y.-H., Chang, K.-S., Chen, C.-Y., Hsu, C.-L., Chang, T.-C., Jang, H.-D. (2018) Enhancement of the Efficiency of Bioethanol Production by Saccharomyces cerevisiae via Gradually Batch-Wise and Fed-Batch Increasing the Glucose Concentration, *Fermentation*, 4(2), 45, DOI: 10.3390/fermentation4020045.

[81] Khongsay, N., Laopaiboon, L., Jaisil, P., Laopaiboon, P. (2012) Optimization of Agitation and Aeration for Very High Gravity Ethanol Fermentation from Sweet Sorghum Juice by Saccharomyces cerevisiae Using an Orthogonal Array Design, *Energies (Basel).*, 5(3), 561–576, DOI: 10.3390/en5030561.

[82] Kumoro, A.C., Damayanti, A., Shiddieqy Bahlawan, Z.A., Melina, M., Puspawati, H. (2021) Bioethanol Production from Oil Palm Empty Fruit Bunches Using Saccharomyces cerevisiae Immobilized on Sodium Alginate Beads, *Periodica Polytechnica Chemical Engineering*, 65(4), 493–504, DOI: 10.3311/PPch.16775.

[83] Kumoro, A.C., Damayanti, A., Shiddieqy Bahlawan, Z.A., Melina, M., Puspawati, H. (2021) Bioethanol Production from Oil Palm Empty Fruit Bunches Using Saccharomyces cerevisiae Immobilized on Sodium Alginate Beads, *Periodica Polytechnica Chemical Engineering*, 65(4), 493–504, DOI: 10.3311/PPch.16775.

[84] Orrego, D., Zapata-Zapata, A.D., Kim, D. (2018). Ethanol production from coffee mucilage fermentation by S. cerevisiae immobilized in calcium-alginate beads, *Bioresour. Technol. Rep.*, 3, 200–204, DOI: 10.1016/j.biteb.2018.08.006.

[85] Duarte, J.C., Rodrigues, J.A.R., Moran, P.J.S., Valença, G.P., Nunhez, J.R. (2013) Effect of immobilized cells in calcium alginate beads in alcoholic fermentation, *AMB Express*, 3(1), 31, DOI: 10.1186/2191-0855-3-31.

[86] Kumoro, A.C., Damayanti, A., Shiddieqy Bahlawan, Z.A., Melina, M., Puspawati, H. (2021) Bioethanol Production from Oil Palm Empty Fruit Bunches Using Saccharomyces cerevisiae Immobilized on Sodium Alginate Beads, *Periodica Polytechnica Chemical Engineering*, 65(4), 493–504, DOI: 10.3311/PPch.16775..